UC Berkeley
UC Berkeley Electronic Theses and Dissertations

Title

Virally-mediated disruption of cellular homeostasis: regulation of pH and HDAC function

Permalink

Author

Vargas-Zapata, Valerie Yaitza

Publication Date

2022

Peer reviewed|Thesis/dissertation

Virally-mediated disruption of cellular homeostasis: regulation of pH and HDAC function

By

Valerie Y. Vargas-Zapata

A dissertation submitted in partial satisfaction of the

requirements for the degree of

Doctor of Philosophy

in

Molecular and Cell Biology

in the

Graduate Division

of the

University of California, Berkeley

Committee in charge:

Professor Laurent Coscoy, Chair
Professor Britt Glaunsinger
Professor Gregory Barton
Professor David Raulet

Fall 2022

Abstract

Virally-mediated disruption of cellular homeostasis: regulation of pH and HDAC function

by

Valerie Y. Vargas-Zapata

Doctor of Philosophy in Molecular and Cell Biology

University of California, Berkeley

Professor Laurent Coscoy, Chair

Viruses have evolved to manipulate the cellular environment to promote their replication and spread. They do so by encoding viral effectors that co-opt or disrupt cellular processes to create an environment suitable for infection. This dissertation will discuss on two viral proteins that disrupt cellular homeostasis. First, I will present work demonstrating that the SARS-CoV-2 Envelope (E) protein interferes with retention of the endoplasmic reticulum (ER) aminopeptidase associated with antigen processing (ERAAP) in cells. To protect the SARS-CoV-2 fusion protein Spike from improper cleavage by Golgi resident proteases, E protein increases the pH of this compartment. The change in pH delays trafficking and likely impairs the function of these proteases. We show that E-mediated Golgi pH neutralization impedes ERAAP retention likely by disrupting the interaction between ERAAP and ERp44, a chaperone we and others have shown to control ERAAP localization. Specifically, we demonstrate that the expression of SARS-CoV-2 E results in decreased ERAAP intracellular levels and ERAAP secretion into the extracellular environment. ERAAP's reliance on ERp44 and a functioning ER/Golgi pH gradient for proper localization and function led us to propose that ERAAP serves as a sensor of disturbances in the secretory pathway during infection and disease.

The second viral protein that will be discussed is the M18 protein from murine cytomegalovirus (MCMV). Previous work found that M18 disrupts the function of histone deacetylases (HDACs). HDACs are epigenetic modulators capable of controlling gene expression by removing acetyl modifications on histones and non-histone proteins. Importantly, HDACs have been shown to regulate herpesvirus replication and latency. Moreover, herpesviruses encode proteins that antagonize or harness the action of these enzymes. I aimed to elucidate the cellular functions of M18 and the contribution of this protein to viral pathogenesis. Here, we demonstrate that M18 is produced as two isoforms, M18L and M18S, during infection. These isoforms likely possess different functions, as suggested by their differential localization. Furthermore, using RNAseq, we found that M18 regulates the expression of a subset of immune-related genes, including various members of the chemokine family. We hypothesize that induction of these factors by M18 could promote viral dissemination by recruiting monocytes, which are known MCMV reservoirs.

Altogether, this dissertation presents work that expands our understanding of viral effectors and their cellular functions. These contributions further illuminate the complex interactions between viruses and their hosts.

Table of Contents

Dedication

A mis padres: Elizabeth Zapata y Félix Vargas y a mi hermana Nathalie Vargas Zapata. Este trabajo se los dedico a ustedes. Sin ustedes esto no hubiese sido posible. Gracias por su amor y por siempre creer en mí. Gracias por siempre apoyarme desde la distancia.

Acknowledgments

I want to first thank my mentor, Laurent Coscoy for his guidance and support. This has been a difficult journey and I appreciate you believing in me. Thank you to my thesis committee members, Greg Barton, David Raulet, and Britt Glaunsinger, for their ideas and support. To the Coscoy lab members, past and present, thank you for all your help, mentorship, and for being my science companions. I want to acknowledge those with whom I shared most of this journey: Allie, Kristi, Jessica, and Asha; thank you for making my time in the lab fun and for all your encouragement, ideas, and help. To Asha Pappajohn: thank you for the opportunity to be your mentor. You were my first lab undergraduate mentee, and I will always remember you fondly. I am rooting for you! I want to also thank all the members of the Glaunsinger lab. Thank you for all your insightful ideas and suggestions. To Britt: thank you for always making me feel welcomed in our joint lab meetings and cared for during my thesis committee meetings. I want to thank some Glaunsinger lab members and alumni which have been bothered by me and have been generous with their help and time: Ella, Jessica, Michael, Aaron, Azra, and Leah. I would also like to thank the QFL team for your enthusiasm and ideas.

In my time at Berkeley, I had the opportunity to be part of various groups through which I found community and purpose. Thank you to the Underrepresented Researchers of Color (UROC) community. Being a coordinator for this program has been an honor and a highlight of my time at Berkeley. To Sean Burns: thank you for believing in me and giving me the opportunity to be a UROC coordinator. To Jessica Stevenson Steward: thank you for trusting me, and for all your encouragement and support. To all the UROC coordinators, past and present: thank you for intentionally creating a space where we could encourage and support each other. Thank you to the inclusive MCB community for allowing me to meet people with a shared set of values and commitment to making academia a more inclusive place for all. To my Boricuas in Berkeley: gracias por su calor, por el espacio para ser quien somos, y por la oportunidad de crear comunidad en Berkeley.

To my Berkeley mom, Audrey Knowlton: thank you for always taking care of Rafael and me, for believing in us, and for all your mentorship and support.

Gracias a mis padres, Félix y Elizabeth, y a mi hermana Nathalie por su amor y apoyo incondicional.

A Raphie: gracias por tu amor, por tu apoyo y por recorrer este camino conmigo. Estoy agradecida de tenerte a mi lado hasta en los momentos más oscuros. Gracias por motivarme a estudiar biología y creer en mí. Gracias a Seattle por llegar a nuestras vidas en el momento oportuno, por todos los cuddles y por todo el amor.

A mis amigas Lee, Emma y Angélica: gracias por su amor, por siempre estar ahí para mí cuando más lo he necesitado y por su apoyo incondicional. Angélica: gracias por las citas semanales a tomar café y compartir conmigo las frustraciones de escuela graduada. Michael: gracias por decidir venir a Berkeley y por estar ahí para compartir frustraciones del lab y darnos apoyo.

To Bangtan Sonyeondan (BTS): I discovered your music in 2021. Thank you for bringing me comfort in this last stretch of my PhD. Thank you for being a constant source of inspiration, peace, and happiness in my life. Borahae!

I

Chapter I: Introduction

1.1 Viruses disrupt cellular homeostasis

Viruses are obligate intracellular pathogens that rely on their host for replication and dissemination. Because of this intrinsic link between viruses and their host, viruses have evolved to co-opt and manipulate the cellular environment to fit their needs. Viruses need to replicate successfully, generate viable progeny, and disseminate to neighboring cells, all while trying to avoid immune recognition [1]. In turn, cells have evolved a myriad of mechanisms that allow them to sense virally-mediated disruptions [2]. The activation of these cellular sensing pathways typically results in cell death and/or signals that promote immune recognition and elimination of the infected cell. The study of the strategies that viruses use to target different cellular pathways has yielded fundamental knowledge on how these processes work in normal cells.

This introduction will discuss two aspects of cellular homeostasis and regulation. First, I will address how pH homeostasis is established in the secretory pathway, with an emphasis on the Golgi. The pH gradient of the secretory pathway regulates protein trafficking, sorting, and the acquisition of post-translational modifications, like glycosylation, for proteins and lipids [3]. Maintaining ion concentrations and the resulting pH along the secretory pathway is integral to the normal functioning of the cell. Interestingly, viruses across many families have evolved to disrupt cellular ion gradients [4]. These viral proteins are collectively known as viroporins and will be discussed below. This section serves as an introduction for chapter 2 where I will discuss how one of these viroporins, the envelope (E) protein from Severe Acute Respiratory Syndrome Coronavirus 2 (SARS-CoV-2), interferes with the retention of an enzyme involved in antigen processing by neutralizing the Golgi lumen.

The second aspect addressed in this introduction is the regulation of cellular transcription by histone deacetylases (HDAC). HDAC are enzymes that remove acetyl groups from histones which drives chromatin into a closed, less accessible state[5]. They also regulate a myriad of cellular processes through their effect on non-histone targets[6]. Furthermore, these enzymes do not only serve to regulate cellular transcription, but they also play a role during viral infections[7]. Relevant to this work is their involvement in herpesvirus infection. Examples of how HDAC function is altered during herpesvirus infection and the viral proteins involved in this process will be presented. Chapter 3 will focus on M18, a viral HDAC inhibitor encoded by murine cytomegalovirus (MCMV), and our attempts to learn more about the cellular functions of this protein.

1.2 pH regulation in the secretory pathway

The pH gradient of the secretory pathway is essential for the normal trafficking, sorting, and deposition of post-translational modifications that occur within these compartments. In this system, the pH decreases from the center of the cell toward the plasma membrane. The ER has an almost neutral pH that matches that of the cytoplasm. The Golgi represents an increasingly acidic compartment, with the cis-Golgi (closest to the ER) having an estimated pH of 6.6 and the

trans Golgi network (TGN) (farthest from the ER) reaching a pH of 6.0 [8]. Despite the importance of the Golgi and its functions, the factors regulating the establishment and maintenance of its pH are not entirely understood. Here, I will summarize three main determinants of the resting Golgi pH.

The pH is determined by the concentration of hydrogen ions (H^+) present in solution. Import of H^+ into the lumen of the Golgi is accomplished by the vacuolar ATPase (v-ATPase). The v-ATPase is a multi-subunit complex that uses ATP hydrolysis to fuel the import of H^+ from the cytosol into the Golgi lumen. The v-ATPase does not exclusively localize to the Golgi, and it also participates in the acidification of other endocytic and secretory compartments [9]. However, numerous isoforms of the subunits have been identified in different compartments, and cell types. These differences are thought to contribute to the specific localization and function of the v-ATPases [10]. Glucose availability has also been shown to regulate the assembly and disassembly of this complex, but under normal conditions, it is thought that the Golgi v-ATPase is constitutively active. Indeed, when the v-ATPase is inhibited by treatment with concanamycin A, the pH gradient of the Golgi is disrupted, and the pH steadily increases in this compartment[11], suggesting constant H^+ import. Interestingly, experiments where cells were permeabilized and excess ATP was added showed a rapid acidification of the Golgi that was well below (~pH 5.0) the physiological levels observed in cells[11]. This suggests that acidification of the Golgi by the v-ATPase needs to be counteracted to maintain the steady-state pH of this compartment.

If H^+ import into the Golgi lumen was not counteracted, the membrane potential would change due to the accumulation of positive charge inside the Golgi. Two main mechanisms exist to counteract the action of the v-ATPase: counterion conductance and proton leak[8,11]. Counterion conductance refers to the import of anions like chloride (Cl^-) or the efflux of cations like potassium (K^+). Maeda, *et. al* identified the Golgi pH regulator (GPHR), a Cl^- channel, as a significant contributor to the Golgi pH. GPHR mutant cells showed impaired transport and glycosylation. Importantly, silencing of GPHR by siRNA resulted in an increase of the steady state pH of the Golgi, and GPHR was shown to not affect lysosomal pH[12]. Two other Golgi anion channels, GOLAC-1 and GOLAC-2, have also been identified[13,14], but some have suggested that they might be the same channel as GPHR[15]. In addition, other ion channels have been shown to localize to the Golgi, but their role in pH regulation of this organelle is unclear. The high permeability of the Golgi to K^+ has led to the proposal that K^+ efflux might also contribute to counterion conductance[16]. However, the role of specific K^+ transporters in maintaining steady state Golgi pH in normal cells is not fully understood[11].

Proton leak represents the third main determinant of the Golgi pH. Proton leakage becomes evident when the v-ATPase is inhibited. As mentioned above, inhibition with concamycin A results in an increase in Golgi luminal pH, suggesting dissipation of H^+ ions[3,11,16]. The process of H^+ leakage is essential as it prevents over-acidification of the Golgi. At steady state, the rate of H^+ leakage matches that of H^+ influx by the v-ATPase. Furthermore, it has been shown that the H^+ leakage rate of the ER is different from that of the Golgi, suggesting that this process helps set the resting pH of these compartments and establish the pH gradient of the secretory

3

pathway[17]. Evidence supports the existence of a Golgi H^+ exporter, but its identity remains elusive. Another process that might contribute to lowering the concentration of H^+ in the Golgi luminal space is through existing Golgi buffering systems. For example, it has been shown that bicarbonate (HCO_3), which can enter the Golgi through the HCO_3/Cl^- anion exchanger SLC42A, can serve this role[18]. In the presence of H^+, HCO_3 can convert into carbonic acid before further breaking into CO_2 and H_2O. Both CO_2 and H_2O can then exit into the cytoplasm by diffusion or aquaporins, respectively.

The three components mentioned here help set the steady state pH of the Golgi and other compartments within the secretory pathway. Abnormalities in the resting pH of the secretory pathway and pH regulation pathways have been observed in cancer cells and specific diseases[11]. Relevant to this dissertation is the dysregulation of pH caused by viruses through encoded ion channels named viroporins.

1.3 Viroporins

Viroporins are small hydrophobic ion channel-like proteins. This family of proteins is encoded by an expanding number of RNA and DNA viruses across many different families, including some of clinical importance like Influenza A Virus (IAV), Human Immunodeficiency Virus (HIV), Hepatitis C Virus (HCV), and SARS-CoV-2[19,20]. Viroporins play a diverse and crucial role in the viral life cycle and pathogenesis. Many of these proteins facilitate replication by participating in steps like viral assembly, budding, and release from cells. This has made them of interest as potential therapeutic targets[19]. Viroporins can have different topologies, but they all contain a transmembrane domain that lets them insert into membranes. This feature allows them to form pores upon oligomerization, which can result in alterations to ion gradients in the cell[4]. Viroporins do not typically display strong ion selectivity but generally prefer cations (i.e., H^+, K^+, Ca^{2+}). Through their varied functions, viroporins have been shown to exert a range of physiological effects in the cell, including changes in membrane permeability, induction of apoptosis, and inflammasome activation[19,21].

The most studied viroporin is the M2 protein from IAV. M2 is a multifunctional pH-regulated ion-channel that promotes the acidification of the viral core which results in the release of the viral RNA and replication machinery into the cytoplasm of host cells[22]. M2 also localizes to the Golgi membranes where it neutralizes the pH of this organelle[23–26]. For M2, modulating Golgi pH helps protect hemagglutinin (HA) from preemptively adopting the low pH conformation needed for fusion[25]. The p7 protein from HCV has also been shown to disrupt H^+ gradients and increase intracellular pH[27]. Relevant to our work is the ability of the SARS-CoV-2 E protein to also neutralize the Golgi lumen[28]. Envelope has been shown to prevent abnormal processing of the Spike (S) protein[26,29]. Furthermore, a recent study showed that SC2 E promotes retention of S by slowing down trafficking through the secretory pathway, which prevents cell-to-cell fusion[29].

E is one of the 4 main structural proteins from coronavirus. The E protein from SC2 shares over 90% homology with that of SARS-CoV-1[30]. Like other viroporins, E oligomerizes in the ER-Golgi intermediate compartment (ERGIC), forming an ion-conductive pore that shows a preference for cations[31]. E participates in viral assembly by promoting budding through its interaction with the Membrane (M) protein[32,33]. E has also been shown to interact with various host proteins, including Bcl-xL, PALS1, syntenin, sodium/potassium (Na+/K+) ATPase α-1 subunit, and stomatin[32]. Importantly, E has emerged as a significant pathogenesis factor. Viruses lacking E are attenuated[34,35]. E's ion channel-like activity seems to be particularly important. Indeed, a virus encoding an E that lacks ion channel activity accumulates compensatory mutations that restore activity in cells and mice[36]. Furthermore, administration of E alone is sufficient to induce pathology and trigger an inflammatory response resembling acute respiratory distress syndrome in mice[37]. Despite the clear importance of SC2 E in viral pathogenesis, much remains to be known about the cellular functions of this protein.

1.4 HDAC regulation of gene expression

Chromatin is tightly packaged into nucleosomes composed of DNA wrapped around a histone octamer, which consists of two copies of the 4 core histones: H2A, H2B, H3, and H5. Each core histone possesses an N-terminal tail where a variety of post-translational modifications (PTMs) can occur[38,39]. These PTMs control the stability of the nucleosome while also serving as scaffolds for the recruitment of chromatin modifying enzymes[38]. One of the PTMs involved in transcriptional regulation is acetylation. Specifically, the acetylation of lysine residues within H3 and H4 has been extensively studied. One of the ways acetylation contributes to a permissive chromatin state is by promoting relaxation of the nucleosome[40,41]. The negative charge of the acetyl group weakens the interaction between the histones and the DNA, promoting a more relaxed, permissive chromatin state. This reaction is reversible; removal of acetyl groups is associated with a more compact chromatin state. The deposition of acetyl groups on histones and their removal is controlled by the action of histone acetyltransferases (HATs) and histone deacetylases (HDACs), respectively[42] (Figure 1.1). Although HATs are generally thought of as activators and HDACs as repressors, there is certainly more complexity to this mode of epigenetic regulation. Thus, the balance between the action of HATs and HDACs controls the acetylation landscape and transcriptional outcome[41,43,44].

HDAC are highly conserved enzymes. They are divided into 4 distinct classes: I, II, III, and IV. Class I and II HDACs include the classical HDAC1-10[5,45]. While histone acetylation/deacetylation generally controls chromatin accessibility, deacetylation of non-histone proteins has a variety of effects[5,6]. HDACs do not bind to DNA directly but act on DNA through interaction with other cellular factors or as components of repressive complexes. Class I HDACs (HDAC1, HDAC2, HDAC3, and HDAC8) localize to the nucleus, and transcription factors represent important non-histone targets of these enzymes[6]. In addition, Class I HDACs have also been shown to be part of 4 main repressive complexes: Sin3, NuRD, CoREST, and MiDac[5,45]. These complexes regulate numerous cellular processes, including transcription, cell cycle progression, and

differentiation[45]. Through their action on histones or their regulation of non-histone proteins, HDACs have emerged as essential regulators of diverse cellular processes.
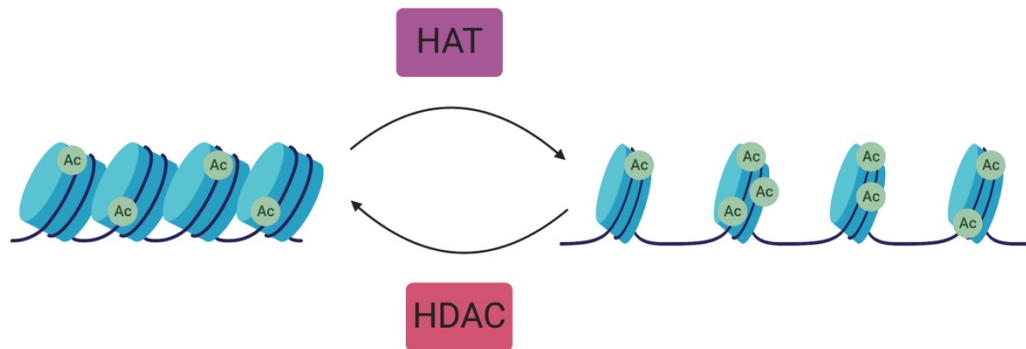

Figure 1.1: **Acetylation regulates chromatin accessibility**. Chromatin condensation is regulated by acetylation. Deposition of acetyl groups on histone tails by Histone acetyltransferases (HATs) promotes a more open, accessible chromatin state. In contrast, removal of these acetyl modifications by Histone deacetylases (HDACs) drives chromatin into a more compact configuration associated with repression. Although there is certainly a correlation between the action of these enzymes and the accessibility of chromatin, the effect of HATS and HDACs on transcription is more complex. It is the balance between the action of these enzymes what dictates the acetylation and transcriptional state of particular loci. Figure created in BioRender.com.

1.5 HDACs in herpesvirus infection

Herpesviruses are enveloped double-stranded DNA viruses. Viruses from the *Herpesviridae* family have been identified in a wide range of animals, including humans. This family can be further divided into three sub-families: *alphaherpesvirinae*, *betahespersvirinae*, and *gammaherpesvirinae*, with human herpesviruses (HHVs) represented in each group[46]. Virtually all humans are infected or will become infected with one or more of these herpesviruses. These infections are typically asymptomatic but can be severe in infants and immunocompromised individuals[47]. HHVs of clinical importance are found in all three subfamilies and include Herpes simplex virus 1 and 2 (HSV-1 and HSV-2), Varicella zoster virus (VZV), human cytomegalovirus (HCMV), Epstein-Barr virus (EBV), and Kaposi's sarcoma-associated herpesvirus (KSHV)[48]. Herpesviruses are highly adapted to their host due to millions of years of co-evolution. This co-evolution has allowed them to develop complex strategies to manipulate the host cell and subvert immune recognition.

The hallmark of herpesviruses is their ability to establish life-long infections in their host. Once herpesviruses infect a cell, they enter the lytic phase of infection where they replicate and produce viral progeny that can infect neighboring cells. This lytic infection is characterized by a coordinated viral gene expression program that allows for the temporal expression of immediate early, early, and late genes. Herpesviruses can then enter a dormant state called latency where their genomes are repressed, little viral replication occurs, and no virions are produced[49,50]. This allows the viral genome to persist in cells and the virus to avoid clearance by the immune system. Latency can be interrupted by intermittent episodes of viral reactivation that allow for replication and dissemination. These different stages of the herpesvirus life cycle are tightly regulated, including at the level of the viral genome. Herpesvirus DNA is subjected to similar regulatory mechanisms than mammalian DNA, including epigenetic regulation by HDACs[7,51].

During lytic infection, immediate early proteins act as transcriptional activators that promote the expression of early and late genes. In CMV, the expression of IE products is controlled by the major immediate early protomer (MIEP). The MIEP is subjected to complex regulation by both activators and repressors[52]. The MIEP must overcome initial repression by the host to allow the production of IE products during lytic infection. Then, the MIEP must be re-silenced in later stages of infection and during latency[53]. One of the repressive factors that regulate the MIEP are HDACs. In mice infected with MCMV, HDAC2 and HDAC3 showed a bi-phasic pattern of association with the MIEP. These factors were initially bound to the MIEP following infection, showed a drop in association, and later steadily increased as the infection progressed towards latency[54]. This correlated inversely with signs of promoter activity, like the presence of polymerase II and acetylated histone 4 at the MIEP. As mentioned, overcoming the repression of the viral genome, partially mediated by HDACs, is essential for reactivation. This is supported by the fact that chemical HDAC inhibitors are commonly used to facilitate the reactivation of herpesviruses like KSHV[55] and HCMV[56,57] in tissue culture models.

To establish latency, genomes need to be repressed. In order to escape latency and enter the lytic cycle, this repression must be alleviated. Thus, it is not surprising that herpesviruses have evolved to modulate HDAC function to facilitate viral replication and latency[51]. Various herpesvirus proteins have been shown to target HDACs or HDAC-containing complexes. Herpesviruses from all subfamilies have been shown to encode proteins that interact with HDACs[51]. Here I will highlight examples from HCMV, as that is the human homolog of MCMV.

The IE proteins, IE1 (also known as IE72) and IE2 (also known as IE86), from HCMV have been shown to interact with HDACs. HCMV IE1 and IE2 co-precipitated with HDAC3 in infected cells[58]. Using a promoter activity assay, the authors showed that HDAC3 represses the promoter of the early gene UL44. The presence of IE1 or IE2 helped partially alleviate this repression and restore activity. Furthermore, the addition of HDAC inhibitors rescued the growth of an HCMV mutant deficient for IE1. IE2 was also shown to interact with HDAC2 in infected fibroblasts and, similar to the previous study, this alleviated the HDAC-mediated repression of an early promoter[59]. Interestingly, HCMV also co-opts HDAC activity. UL29/UL28, in association with UL38, interact with the HDAC1-containing NuRD complex to promote the expression of IE genes from the MIEP[60]. As part of the temporal control of herpesvirus gene expression, IE genes must be repressed at later stages of infection. IE2 was shown to negatively regulate the expression of its own promoter, the MIEP, through recruitment of HDAC1 to the promoter's *cis* repression sequence [61]. Altogether, these examples demonstrate that HDACs play diverse and essential roles during different states of the viral life cycle and highlight the importance of viral proteins that can modulate the action of these enzymes.

II

Chapter II: SARS-CoV-2 Envelope-mediated Golgi pH neutralization interferes with ERAAP retention in cells

A version of this chapter has been published in BioRxiv[62]. That work is included here with permission from the corresponding authors.

2.1 Introduction

ER aminopeptidase associated with antigen processing (ERAAP)

The antigen presentation pathway (APP) provides a snapshot of the intracellular environment to surveying immune cells in the form of peptides presented on major histocompatibility (MHC) molecules[63]. This pathway plays a crucial role in the response against viruses and cancers[64,65]. Presentation of foreign peptides (e.g. from viruses) or altered self-peptides (e.g. cancer) presented on MHC-I molecules allows cytotoxic CD8+ T-cells to recognize and kill infected or cancerous cells, respectively. In this pathway, peptide precursors are generated in the cytoplasm by the proteasome and transported into the endoplasmic reticulum (ER) by the Transporter associated with Antigen Processing (TAP)[66]. Once in the ER, peptides are edited to properly fit into MHC-I molecules. This function is accomplished by the ER aminopeptidase associated with antigen processing (ERAAP) in mice and ER aminopeptidase (ERAP) 1 and 2 in humans[67–69]. We will refer to these collectively as ERAP. ERAP belongs to the M1 family of metallopeptidases, and it trims peptides on their amino (N-) terminus to an approximate length of 8-10 amino acids (Figure 2.1A).

ERAP regulates the quality and nature of the peptide repertoire and therefore shapes the resulting immune responses[70,71]. Loss of ERAAP leads to an altered peptide repertoire characterized by changes in the abundance and length of peptide precursors[72]. The peptidome of ERAAP deficient cells is sufficiently different from normal cells that these MHC-I:peptide complexes can elicit an immune response. Indeed, mice immunized with ERAAP KO cells mount a robust CD8+ T-cell response that eliminates these cells[73]. Careful analysis of the responding CD8+ T-cells revealed that most of them recognize FL9 (a self-peptide derived from the ubiquitously expressed host proteins Fam49A and B) that is presented by the non-classical MHC-I molecule, Qa1b. As a result, these cells were named QFL T-cells (Figure 2.1B). Upon recognition of the FL9:Qa1b complex, QFL T-cells can kill target cells and produce inflammatory cytokines[73,74]. So far, FL9 presentation has only been reported in cells experiencing ERAAP dysfunction. Thus, it has been suggested that QFL T-cells serve to monitor ERAAP function and eliminate defective cells.

The existence of QFL T cells has not yet been reported in humans. However, T cell responses restricted to the human homolog of Qa1b, HLA-E, exists and they play an important role in both infectious disease and vaccination[75]. HLA-E can present pathogen-derived peptides to CD8+ T cells and these have been shown to play a protective role in infections with *Mycobacterium tuberculosis*, HIV, and CMV, among others[76,77]. Recent research has focused on the promising role of HLA-E-restricted CD8+ T cells in the context of vaccination. Vaccination studies in rhesus macaques (Rm) using CMV-based vectors revealed that this vaccine platform elicits strong protective and long-lasting memory CD8+ T cell responses restricted to the Rm homolog of HLA-E, Mamu-E[78–81]. Whether a component of these HLA-E-restricted CD8+ T cell responses can be attributed to a QFL-like population remains to be explored and should be an interesting future area of study.

ERAAP downregulation by viruses

Due to the central role of the APP in eliciting antiviral CD8^{+} T-cell responses, many viruses have evolved to disrupt different components of this pathway[64,82], including ERAP. ERAP downregulation was first reported during human cytomegalovirus infection[83]. HCMV-encoded microRNA (miRNA), miR-US4-1, was shown to target ERAP1 transcript for degradation, resulting in lower ERAP1 protein levels. In addition to miR-US4-1, HCMV encodes a second miRNA, miR-UL112-5p, which also targets ERAP1 for degradation[84]. Importantly, the authors showed that ERAP downregulation by these miRNAs prevented the generation of HCMV antigenic peptides, thus highlighting the relevance of ERAP targeting as an immune evasion strategy.

Recently, our group showed that infection with MCMV also results in ERAAP downregulation[85]. MCMV-infected cells show a drastic loss of ERAAP protein levels. In contrast to what was observed with HCMV, ERAAP mRNA levels were not altered in MCMV-infected cells. The mechanism behind ERAAP downregulation during MCMV infection is not entirely understood. Follow-up experiments by Kristina Geiger in our lab demonstrated that ERAAP downregulation is likely caused by an early viral protein and does not involve miRNAs encoded in the m01-22 genomic region of MCMV. Screening to identify viral proteins that could be responsible for ERAAP downregulation yielded multiple candidates. This suggested that the mechanism at play during MCMV infection potentially involves multiple viral proteins. It is also possible that ERAAP downregulation is the result of changes to the cellular state during infection.

Interestingly, loss of ERAAP during MCMV infection triggers a QFL T-cell response[85]. ERAAP loss in this context allows for the presentation of the QFL activating ligand, FL9: Qa1b complex. In MCMV-infected mice, QFLs proliferate and produce inflammatory cytokines like Interferon-γ. Furthermore, QFL T-cells contribute to viral restriction. In a bone marrow transfer experiment, immunodeficient mice (Rag2$^{-/-}$, γC$^{-/-}$; which lack lymphocytes) that were injected with QFL T-cells showed lower viral titers in the spleen and liver in comparison to mice that received an irrelevant T-cell clone. These exciting observations suggested that the immune system could recognize ERAAP dysfunction in the context of infection.

Project rationale

Given the significance of ERAAP's function and the consequences of its loss, we became interested in the cellular pathways that regulate ERAAP in normal cells and whether those could be disrupted during viral infection. Here we show that ERp44 promotes ERAAP retention in the ER, a process regulated by the pH of the ER and Golgi. We demonstrate that the Envelope (E) protein from Severe Acute Respiratory Syndrome Coronavirus 2 (SARS-CoV-2) increases the Golgi pH, leading to a decrease in ERAAP intracellular protein levels and its release into the extracellular environment. Because E's ability to modulate ion gradients is part of SARS-CoV-2's life cycle and pathogenesis, we propose that ERAAP could be an indicator of the integrity of the secretory pathway, and its loss and/or secretion could signal an altered cellular state like viral infection.

11

The data presented in this chapter is reproduced from the manuscript that I co-authored with Kristina Geiger[62]. The contributions of other authors will be highlighted in the text or figure legends.

2.2. Results

ERAAP dsRed is expressed and properly localized to the ER

Our lab recently described that cells infected with MCMV express low levels of ERAAP[85]. Through this work, we became interested in identifying the cellular pathways that regulate ERAAP protein levels in cells under normal conditions and determining whether these pathways could be targeted during viral infection. To address this question, we performed a genome-wide CRISPR KO screen to identify host factors that regulate ERAAP levels in cells. To this end, a reporter cell line that expresses an ERAAP-dsRed fusion protein was generated to allow the monitoring of ERAAP levels by flow cytometry. Human Burkitt lymphoma B (BJAB) cells were transduced to express ERAAP-dsRed and subsequently two cell clones (B2 and D4) that possessed homogenous, stable, and high expression of ERAAP-dsRed were isolated (Figure 2.2A).

To confirm the proper ER localization of the ERAAP-dsRed construct, an Endoglycosidase H (Endo H) assay was performed. Glycans added to proteins in the ER are further modified as they transit through the Golgi. These modifications change the sensitivity of the glycan structure to cleavage by enzymes like Endo H. Thus, Endo H sensitivity can be used as an indicator of the general localization within the secretory pathway. ERAAP resides in the ER and should remain sensitive to Endo H cleavage. Indeed, ERAAP-dsRed shows sensitivity to Endo H cleavage as evidenced by the appearance of a lower molecular weight band (shift from ~150 kDa to 130 kDa) in samples treated with the enzyme in comparison to untreated samples (Figure 2.2B). Endogenous ERAP was also detected in this gel (~100 kDa) and remained Endo H sensitive suggesting ERAAP-dsRed expression does not interfere with the localization of the endogenous protein. Since both cell clones showed high expression of ERAAP-dsRed and proper ER localization, we selected clone B2 to perform our experiments.

ERp44 regulates ERAAP levels

To perform the genome-wide CRISPR KO screen, BJAB ERAAP dsRed cells (clone B2) were transduced to express Cas9. These cells were then transduced with the human genome-scale CRISPR KO (GeCKO) v2 library targeting over 19,000 genes (containing 6 guide RNAs (gRNAs) per gene). After selection and recovery, cells with the top and bottom 10-15% dsRed signal were sorted. The gRNAs present in these cell populations were identified by sequencing and compared for gene enrichment.

From our hits, ERp44 stood out for its role in modulating the localization and trafficking of different host proteins[86]. Other potential hits obtained from the gRNA library screen mostly corresponded to proteins involved in transcriptional regulation (Figure 2.3). Because of the high likelihood that these factors control ERAAP dsRed transcription from the CMV promoter of our retroviral construct, we decided to only focus on ERp44 in this study.

ERp44's interaction with ERAP has been reported to regulate ERAP localization by retrieving it from the ER-Golgi intermediate compartment (ERGIC)/cis-Golgi and bringing it back into the ER[87]. To confirm the results of our screen, BJAB ERAAP dsRed cells were transduced with a gRNA targeting ERp44. As expected, cells lacking ERp44 showed a marked decrease in ERAAP protein levels, as observed by western blot (Figure 2.4A) and by flow cytometry (Figure 2.4B). Knockout of ERAAP did not affect ERp44 levels (Figure 2.4A).

To test if ERAAP was being secreted from BJAB cells lacking ERp44, ERAAP was immunoprecipitated from the supernatant and ERAAP activity was quantified using the leucine aminopeptidase (LAP) activity assay[87]. As predicted, ERp44 KO cells secreted ERAAP as evidenced by increased LAP activity compared to parental cells (Figure 2.4C). ERp44 controls ERAAP retention across a variety of cell lines, both mouse (Figure 2.5) and human[87] (Figure 2.4C) suggesting ERp44's regulation of ERAP is a conserved feature of mammalian cells.

SARS-CoV-2 Envelope neutralizes the pH of the Golgi

One of the factors regulating ERp44's function is pH. Dysregulation of the Golgi pH abrogates the ability of ERp44 to interact with its clients and results in their secretion[88]. We reasoned that interfering with the pH homeostasis of the Golgi could have negative consequences for ERAAP function. Interestingly, some viruses encode proteins that modify the pH of intracellular compartments as part of their viral life cycle[4]. In particular, the E proteins from the coronaviruses Infectious Bronchitis virus (IBV) and SARS-CoV-2 have been shown to increase the pH of the Golgi[26,28]. Neutralization of the Golgi space is thought to protect the fusion protein Spike (S) from abnormal cleavage by Golgi resident proteases[26,89]. E oligomerizes into an ion-conductive pore and is involved in viral assembly, budding, and pathogenesis[32,35]. Viruses lacking E are attenuated[33,34] and E's ion channel-like activity seems particularly important for pathogenesis and SARS-CoV-2-induced pathology[36,37]. Still, much remains to be known about E's intracellular function and impact on cellular pathways.

We hypothesized that during SARS-CoV-2 infection, E-mediated neutralization of the Golgi and the subsequent loss of ERp44 activity might result in ERAP being secreted rather than retained into the ER. We decided to first confirm that the expression of SARS-CoV-2 E in cells indeed causes an increase in the pH of the Golgi as previously reported[28]. To that extent, we used the pH reporter pHluorin-TGN38, a Golgi-localized GFP variant that exhibits bimodal excitation at 405 nm and 488 nm[12]. The fluorescence emission from this reporter changes in response to pH. Specifically, the emission ratio of pHluorin (405 nm/488 nm) increases as pH increases. HeLa cells co-transfected with SARS-CoV-2 E showed a higher pHluorin emission ratio compared to cells transfected only with the reporter (Figure 2.6A). Using HeLa cells transfected with the

13

reporter and resuspended in buffers of known pH, we generated a standard curve to convert pHluorin emission ratios to pH values. As expected, cells expressing SARS-CoV-2 E showed neutralization of the Golgi compared to control cells. In control cells, the pH of the Golgi was 6.9 and increased to 7.4 in cells expressing SARS-CoV-2 E (Figure 2.6B). As an additional control, we transfected cells with Influenza A virus (IAV) M2, a viral protein known to increase the Golgi pH[23–26], and observed an increased pHluorin emission ratio (Figure 2.6A) that translated to a Golgi pH of 7.3 (Figure 2.6B). These data suggest that SARS-CoV-2 E behaves as previously demonstrated by neutralizing the pH of the Golgi.

SARS-CoV-2 Envelope leads to decreased ERAAP levels

Next, we asked if SARS-CoV-2 E expression could result in a reduction in ERAAP's intracellular levels. To evaluate ERAAP levels specifically in cells expressing SARS-CoV-2 E, we decided to use a co-transfection system. HEK293T cells were chosen as they are easily transfectable and express low ERAP levels endogenously. HEK293T cells were co-transfected with a vector encoding ERAAP-dsRed and another vector encoding GFP and SARS-CoV-2 E (or a vector expressing only GFP as control). 24- and 48-hours post-transfection (hpt), cells were harvested and ERAAP dsRed levels were evaluated by flow cytometry. Cells expressing SARS-CoV-2 E showed decreased ERAAP-dsRed levels compared to vector control (Figure 2.7A). Based on the dsRed geometric mean fluorescence for each population, we found that cells expressing SARS-CoV-2 E have ~40-50% of the levels of ERAAP in control cells (Figure 2.7B).

The effect of SARS-CoV-2 E on ERAAP protein levels was also confirmed using an alternative method. Cells were co-transfected with a vector encoding a Flag-tagged ERAAP and a vector encoding SARS-CoV-2 E or an empty vector control. 36 hpt, whole cell lysate (WCL) was collected and ERAAP protein levels were evaluated by western blot. As observed before, cells expressing SARS-CoV-2 E have decreased levels of ERAAP. Importantly, this effect is specific to SARS-CoV-2 E as co-transfecting a different viral protein, SARS-CoV-2 S, did not decrease ERAAP levels (Figure 2.7C). Analysis of ERAAP levels across multiple experiments revealed that cells expressing E have on average ~60% the levels of ERAAP (40% reduction) of cells co-transfected with the empty vector. Cells co-transfected with an unrelated protein showed no decrease in ERAAP levels (Figure 2.7D). Taken together, these results indicate that SARS-CoV-2 E causes a loss in ERAAP levels likely as a result of disrupting ERp44-mediated recycling of ERAAP.

ERAAP is secreted from cells expressing SARS CoV-2 Envelope

We hypothesized that the loss in ERAAP levels observed in cells expressing SARS-CoV-2 E might result from ERAAP release into the supernatant, as described with cells lacking ERp44[87] (Figure 2.4C). To test this, the supernatant of NIH3T3 cells stably expressing ERAAP dsRed and transfected with SARS-CoV-2 E (or empty vector as control) was collected at 48 hpt, and a LAP assay was performed.

In cells expressing SARS-CoV-2 E, we observed ~34% ERAAP secretion relative to ERp44 KO cells (Figure 2.8). Cells co-transfected with empty vector showed ~13% ERAAP release. This

background level of ERAAP secretion is likely due to overexpression of ERAAP in this system which might saturate retention mechanisms[90]. Still, SARS-CoV-2 E induces a significant 2.7-fold increase in ERAAP secretion relative to empty vector control. Importantly, the amount of ERAAP being secreted by SARS-CoV-2 E-expressing cells is probably vastly underestimated in this assay since only ~20-30% of the cells are transfected with SARS-CoV-2 E (Figure 2.9). Together our results suggest that SARS-CoV-2 E disrupts ERAAP function by preventing the efficient retention of ERAAP inside cells and leading to its secretion.
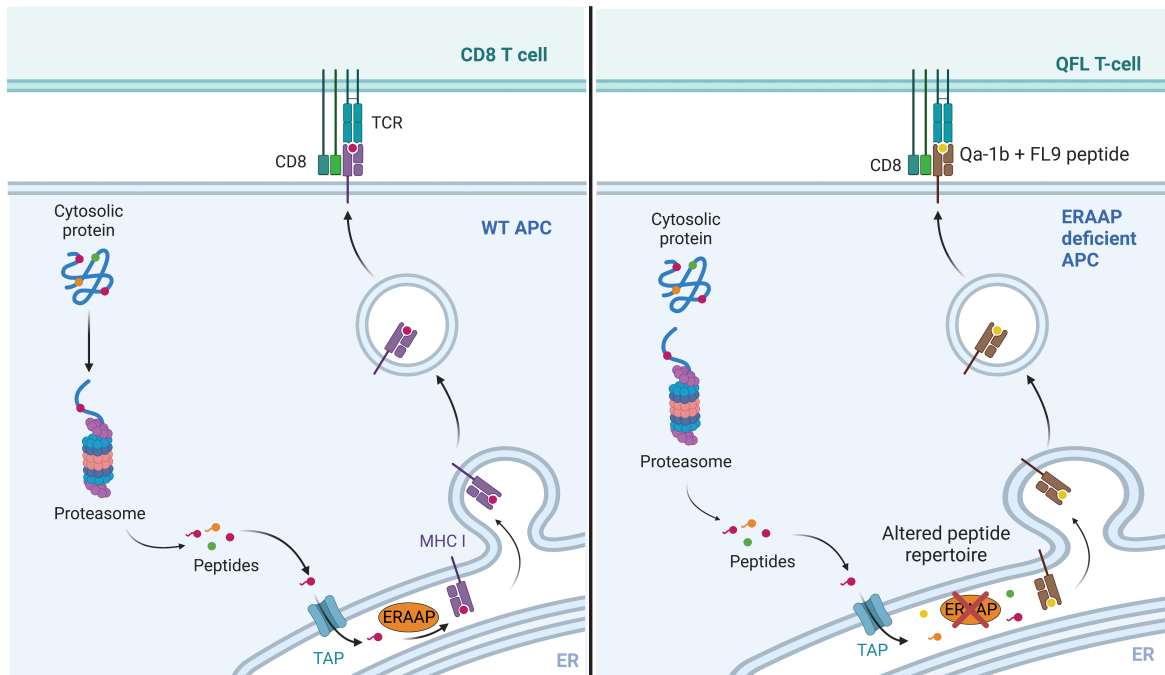
2.3. Figures

Figure 2.1: **Antigen presentation in WT and ERAAP deficient cells**. A. In normal cells, peptide precursors are generated in the cytoplasm by the proteosome. These peptides are imported into the ER by TAP. ERAAP trims peptides to an appropriate length for presentation into MHC-I molecules to surveying CD8$^+$ T-cells. B. ERAAP deficient cells have an altered peptide repertoire. In these cells, novel peptides or peptides with N-terminal extensions can be presented. The FL9 peptide, derived from the Fam49A and B proteins, is presented on Qa1b, a non-classical MHC-I molecule, in ERAAP deficient cells. Presentation of the FL9: Qa1b complex is recognized by a subset of CD8$^+$ T-cells called QFL T-cells, which can kill target cells. Figure created in BioRender.com.
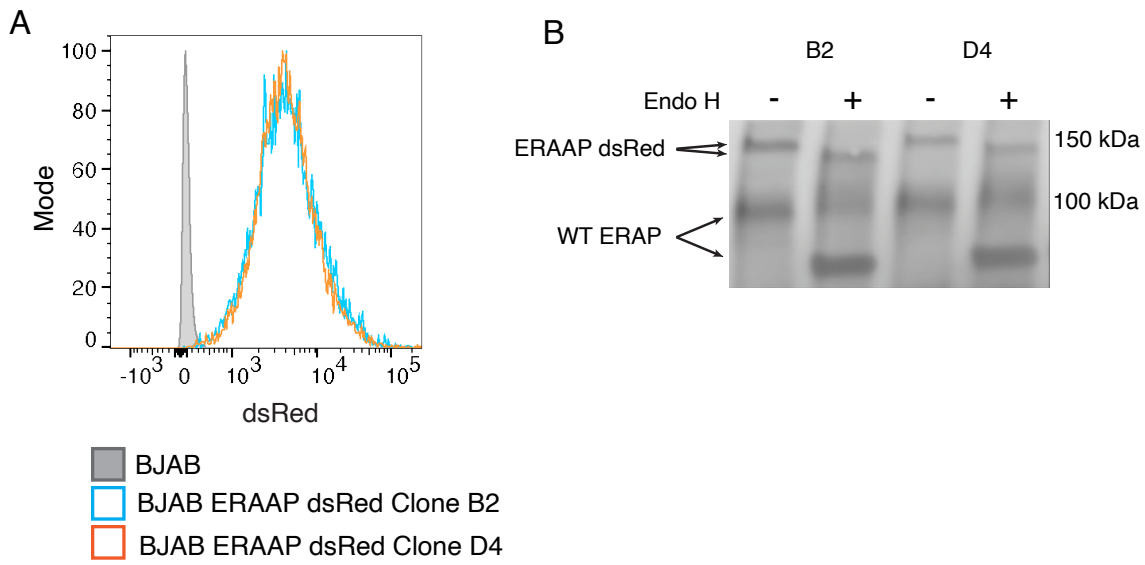
Figure 2.2: **ERAAP dsRed is expressed and properly localized in the ER**. A. BJAB cells were transduced to express an ERAAP dsRed fusion protein. Cells were subcloned and selected for high expression of the construct as measured by flow cytometry. Histogram shows ERAAP dsRed levels in two selected clones, B2 (blue histogram) and D4 (orange histogram), in comparison to non-transduced BJAB cells (grey filled histogram). B. To test for proper ERAAP dsRed localization, Endo H assay was performed. WCL was collected from BJAB ERAAP dsRed clones B2 and D4 and ERAAP was immunoprecipitated using an anti-ERAAP antibody. Purified ERAAP was incubated with Endo H enzyme (Endo H +) or water (Endo H -) as a control. After treatment, ERAAP's molecular weight was determined by western blot. Shown is a representative ERAAP blot. In non-treated samples, ERAAP dsRed appears as a ~150 kDa band (top set of arrows) while endogenous ERAP (WT ERAP; bottom set of arrows) can be observed as a ~100 kDa band. The appearance of a cleavage product of lower molecular weight indicates Endo H sensitivity. Experiment was done by Kristina Geiger.

17

id	num	neg|score	neg|p-value	neg|fdr	neg|rank	neg|goodsgrna	neg|lfc	pos|score	pos|p-value	pos|fdr	pos|rank	pos|goodsgrna	pos|lfc
TRIM28	6	1	0.99999	0.999994	21655	0	12.724	9.7158E-17	2.2861E-07	0.00099	1	6	12.724
ERP44	6	0.99795	0.99793	0.999994	21580	0	11.557	1.2947E-12	2.2861E-07	0.00099	2	6	11.557
SPOP	6	0.99903	0.99902	0.999994	21619	0	8.5488	3.4842E-10	2.2861E-07	0.00099	3	6	8.5488
CCNC	6	0.80567	0.85034	0.999994	17564	1	10.182	1.1113E-08	2.2861E-07	0.00099	4	5	10.182
MGA	6	0.99995	0.99995	0.999994	21652	0	8.2785	7.4993E-08	2.2861E-07	0.00099	5	6	8.2785
PAXIP1	6	0.84935	0.87158	0.999994	18249	1	6.5322	1.6422E-06	9.3729E-06	0.03041	6	5	6.5322
WDR83	6	0.96152	0.96159	0.999994	20620	0	9.1522	1.7951E-06	9.8301E-06	0.03041	7	5	9.1522
ZNF829	6	0.93692	0.93694	0.999994	20004	0	6.7114	3.1646E-06	0.000014859	0.040223	8	4	6.7114
UBE2L3	6	0.86537	0.88052	0.999994	18547	1	5.5462	6.8226E-06	0.000040921	0.091089	9	5	5.5462
UBE2M	6	0.58245	0.727	0.999994	14712	1	8.1294	9.1327E-06	0.000056009	0.110261	10	5	8.1294
CHST9	4	0.99999	0.99999	0.999994	21654	0	8.9971	0.000012035	0.000042064	0.091089	11	4	8.9971
PPP1R13L	6	0.66471	0.78896	0.999994	15854	1	7.7787	0.000016879	0.000099444	0.153819	12	5	7.7787
CXorf38	5	0.99648	0.99645	0.999994	21521	0	5.7248	0.000017008	0.000072011	0.123762	13	5	5.7248
hsa-mir-6807	4	0.86194	0.86157	0.999994	18486	0	9.5479	0.000020798	0.000074297	0.123762	14	3	9.5479
ZNF581	5	0.48471	0.63471	0.999994	13211	1	9.3565	0.00002794	0.00011773	0.169967	15	4	9.3565
USP22	6	0.99997	0.99996	0.999994	21653	0	6.3995	0.000032476	0.00018723	0.238497	16	6	6.3995
MARCH5	5	0.98671	0.9867	0.999994	21269	0	9.3066	0.000033716	0.00014745	0.199567	17	5	9.3066
CELSR1	6	0.018311	0.066506	0.93914	1377	3	3.3324	0.000039051	0.00022381	0.251238	18	3	3.3324
SLC27A5	5	0.33618	0.51061	0.999994	10853	2	9.1782	0.000045813	0.00020918	0.251238	19	3	9.1782
ELP3	5	0.98843	0.98844	0.999994	21312	0	8.3229	0.000050605	0.00023204	0.251238	20	5	8.3229
WDR87	6	0.99955	0.99953	0.999994	21636	0	8.0392	0.000055014	0.0002965	0.272483	21	6	8.0392
C5orf51	6	0.73934	0.82476	0.999994	16728	1	8.4612	0.000055014	0.0002965	0.272483	22	5	8.4612
DDX39B	6	0.86616	0.881	0.999994	18560	1	8.7764	0.000056264	0.00030199	0.272483	23	5	8.7764
RING1	5	0.97609	0.97616	0.999994	20990	0	5.2669	0.000058205	0.00026541	0.272483	24	5	5.2669
HDLBP	6	0.99529	0.99528	0.999994	21487	0	8.7471	0.00006923	0.00037286	0.32297	25	6	8.7471
WDR59	6	0.98335	0.98331	0.999994	21165	0	8.6916	0.000071728	0.0003884	0.323496	26	5	8.6916
GNAS	5	0.92531	0.92555	0.999994	19752	0	9.024	0.000091005	0.00041492	0.332783	27	4	9.024
EIF2S2	5	0.9999	0.99991	0.999994	21651	0	7.8489	0.00010097	0.00044611	0.350119	28	5	7.8489
NIPBL	6	0.9999	0.99989	0.999994	21650	0	7.7534	0.00010138	0.00055803	0.389812	29	6	7.7534
ZBTB45	5	0.24776	0.43902	0.999994	8969	1	8.9864	0.00010276	0.00046887	0.350119	30	4	8.9864
MAP3K14	6	0.99988	0.99987	0.999994	21648	0	7.4638	0.00011415	0.00062387	0.409391	31	6	7.4638
CHUK	6	0.96929	0.96929	0.999994	20809	0	6.3557	0.00011415	0.00062387	0.409391	32	5	6.3557
HMGB1	5	0.99988	0.99989	0.999994	21649	0	7.3593	0.00012066	0.0005482	0.389812	33	5	7.3593
CCND3	6	0.018663	0.067682	0.93914	1397	2	2.5756	0.00014927	0.00081544	0.477254	34	3	2.5756
DENND5A	5	0.99985	0.99986	0.999994	21647	0	6.5204	0.00014984	0.00069977	0.442008	35	5	6.5204
SEC62	5	0.99772	0.9977	0.999994	21571	0	7.7672	0.00015246	0.0007144	0.442008	36	5	7.7672
TMED2	5	0.87892	0.87923	0.999994	18810	1	2.5853	0.00015743	0.00073955	0.444857	37	4	2.5853
PGP	6	0.98503	0.985	0.999994	21223	0	4.3368	0.00016702	0.00091146	0.509901	38	5	4.3368
MED13	6	0.38841	0.59493	0.999994	11773	1	7.8867	0.00017099	0.00093798	0.509901	39	5	7.8867
EMC6	6	0.99695	0.99694	0.999994	21537	0	6.8158	0.00017666	0.00096678	0.509901	40	6	6.8158
SMPDL3A	6	0.99982	0.9998	0.999994	21646	0	4.6863	0.00018148	0.0009869	0.509901	41	6	4.6863
CSTF2	6	0.99981	0.9998	0.999994	21645	0	6.839	0.0001873	0.0010125	0.509901	42	6	6.839
SWT1	5	0.97386	0.9739	0.999994	20922	0	3.1506	0.00021212	0.0010056	0.509901	43	5	3.1506
ZNF644	6	0.99496	0.99495	0.999994	21475	0	6.1815	0.0002128	0.0011346	0.524099	44	6	6.1815
TOX4	6	0.88764	0.89467	0.999994	18990	1	2.9797	0.00021491	0.0011465	0.524099	45	4	2.9797
KDM5C	6	0.99659	0.99656	0.999994	21524	0	5.8398	0.00022239	0.001184	0.524099	46	6	5.8398
MFN1	5	0.85603	0.8591	0.999994	18374	1	8.746	0.00022624	0.0010715	0.524099	47	4	8.746
ZNF345	6	0.91878	0.91927	0.999994	19603	1	2.3618	0.00023441	0.0012461	0.524099	48	4	2.3618
ANGEL1	5	0.95886	0.959	0.999994	20558	0	8.7306	0.00023718	0.0011131	0.524099	49	4	8.7306
RPN2	6	0.99976	0.99974	0.999994	21644	0	6.6867	0.00024009	0.0012827	0.524099	50	6	6.6867
MBOAT7	6	0.99973	0.99971	0.999994	21642	0	8.2125	0.00025404	0.001349	0.532462	51	6	8.2125

Figure 2.3: **Hits identified in genome-wide CRISPR KO screen**. Hits represent gRNAs enriched in BJAB ERAAP dsRed cells expressing low levels of ERAAP dsRed after transduction with gRNA library. BJAB ERAAP dsRed cells with the top or bottom ~10-15% dsRed signal were sorted, analyzed by sequencing, and compared for gene enrichment. Shown is enrichment analysis for cells showing loss of ERAAP dsRed expression in comparison to high expressors. Enrichment analysis was performed using the MaGeCK method. List represents a subset of the hits. Full list can be accessed as supplemental figure 1 in manuscript. Experiment was done by Kristina Geiger and Andreas Puschnik.
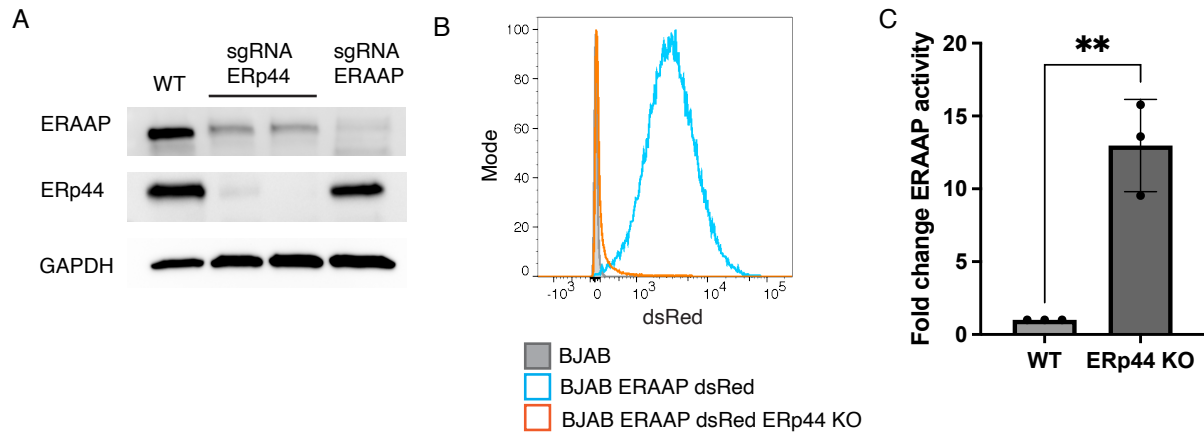
Figure 2.4: **ERp44 regulates ERAAP levels.** A. To confirm the results of the CRISPR KO screen, BJAB ERAAP dsRed cells (clone B2) were transfected with two gRNA targeting ERp44 or one gRNA targeting ERAAP as a control. ERAAP levels in ERp44 KO cells were measured by western blot. Representative blot showing ERAAP and ERp44 protein levels in untransfected BJAB ERAAP dsRed (WT) and KO cells. GAPDH is shown as a loading control. B. Histogram showing ERAAP dsRed levels in BJAB ERAAP dsRed (blue histogram) and ERp44 KO cells (orange histogram). Parental BJAB cells are shown as a control (grey filled histogram) C. ERAAP secretion from ERp44 KO cells was measured by LAP assay. ERAAP was immunoprecipitated from the supernatants of BJAB ERAAP dsRed and BJAB ERAAP dsRed ERp44 KO cells. Beads containing ERAAP were incubated with LpNA substrate and LAP activity was measured 8 h after addition of the substrate by measuring optical density (OD) at 410 nm. Background activity coming from media was subtracted from both conditions. Shown is the fold change in LAP activity relative to BJAB ERAAP dsRed (WT) cells. Data represents mean$\pm$ SD from three independent experiments. Unpaired two-tailed T-test was performed. ** p value < 0.01. Experiments presented in 2.3A and 2.3C were performed by Kristina Geiger with help of Xiaowen Mao and Jessica Ma.
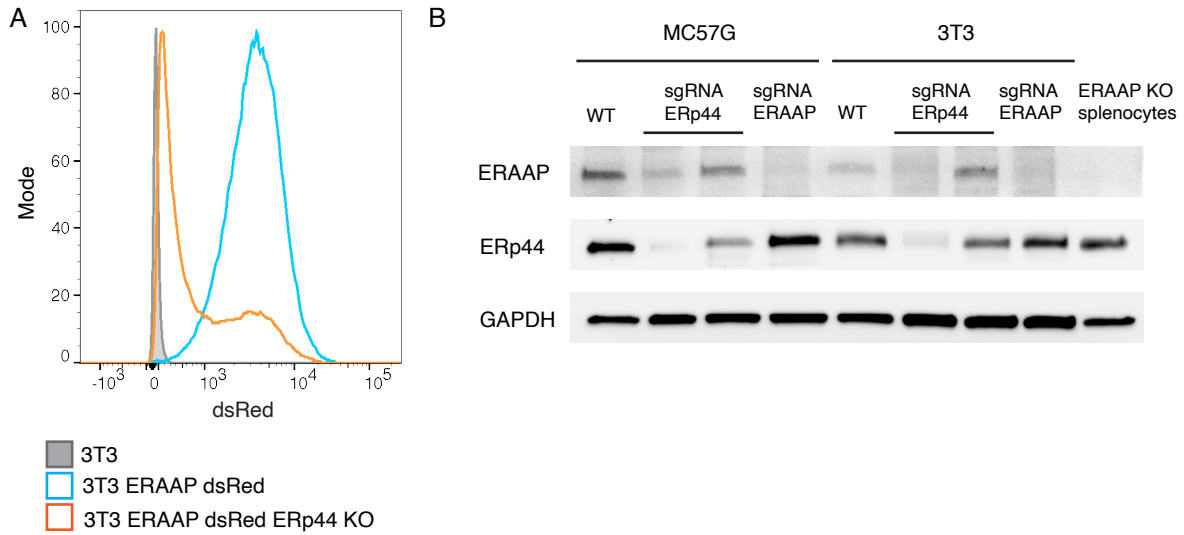
Figure 2.5: **ERp44 regulates ERAAP levels in mouse cells**. A. NIH 3T3 cells were transduced to express ERAAP dsRed and ERp44 was knocked out in this cell line. ERAAP dsRed levels were assessed by flow cytometry. Histogram shows ERAAP dsRed levels in NIH 3T3 ERAAP dsRed (blue histogram) and ERp44 KO cells (orange histogram). Parental NIH 3T3 cells are shown as a control (grey filled histogram). B. MC57G and NIH 3T3 cells were transfected with two gRNA targeting ERp44 or one gRNA targeting ERAAP as a control. ERAAP levels in ERp44 KO cells were measured by western blot. Representative blot showing ERAAP and ERp44 protein levels in untransfected (WT) and KO cells. ERAAP KO splenocytes were included as comparison. GAPDH is shown as a loading control. NIH 3T3 ERAAP dsRed (WT) and ERp44 KO cells used in 2.5A were generated by Dan Tran. Experiment presented in 2.5B was performed by Kristina Geiger with help of Xiaowen Mao.
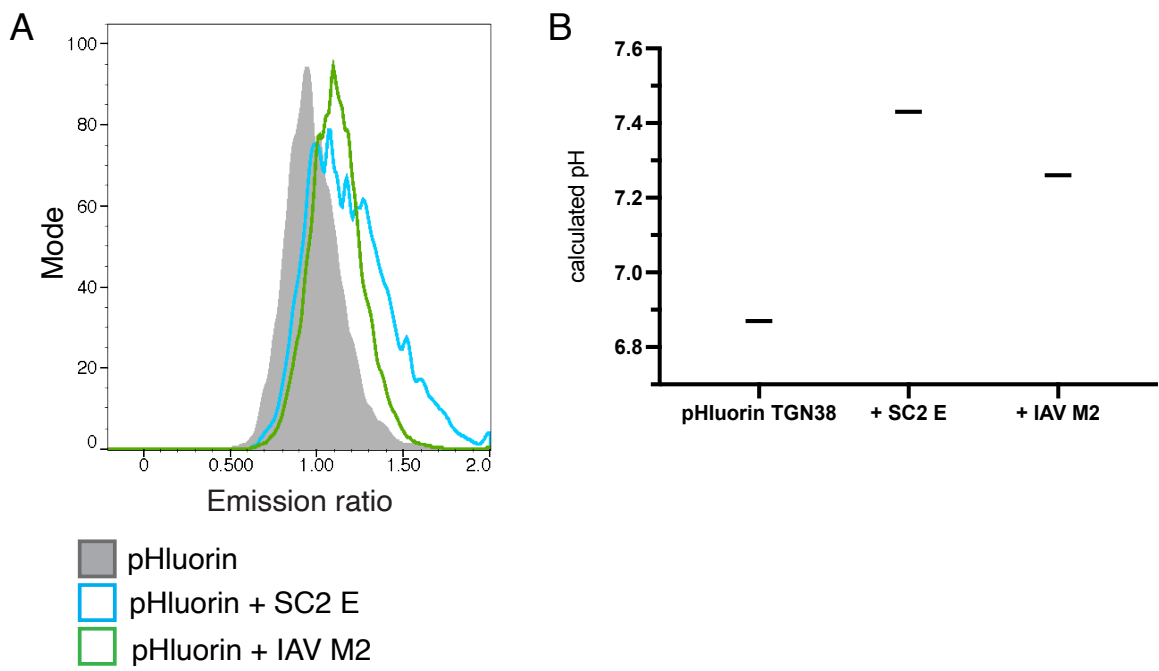
Figure 2.6: **SARS-CoV-2 Envelope neutralizes the pH of the Golgi.** A. Hela cells were transfected with pHluorin-TGN38 alone (grey filled histogram) or co-transfected with pHluorin-TGN38 and SC2 E (blue histogram) or IAV M2 (green histogram). The fluorescence emission of pHluorin-TGN38 was measured by flow cytometry after excitation at 405 nm and 488 nm. Histogram shows the pHIuorin-TGN38 emission ratio (405 nm/488 nm) for each condition. B. Using a pH standard curve, the emission ratios values for each condition were used to calculate the pH of the Golgi. Shown are the calculated pH values for the Golgi space in Hela cells transfected with pHIuorin-TGN38 alone or co-transfected with SC2 E and IAV M2. Data shown is from one representative experiment.
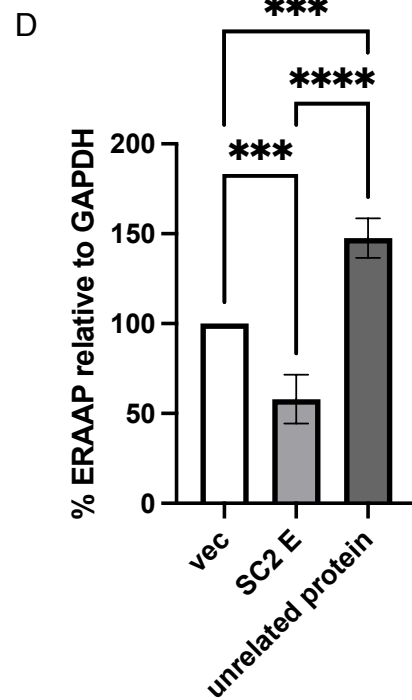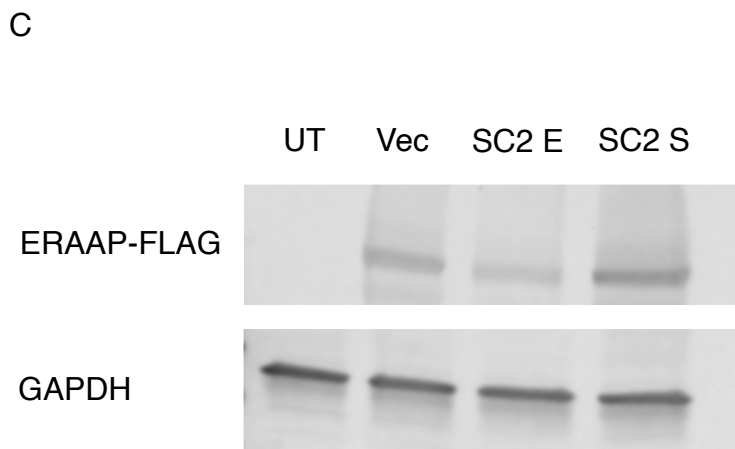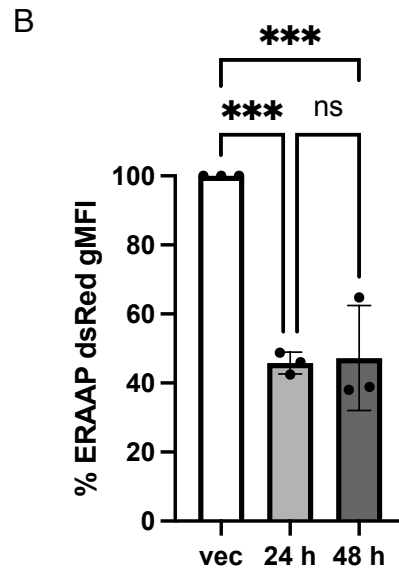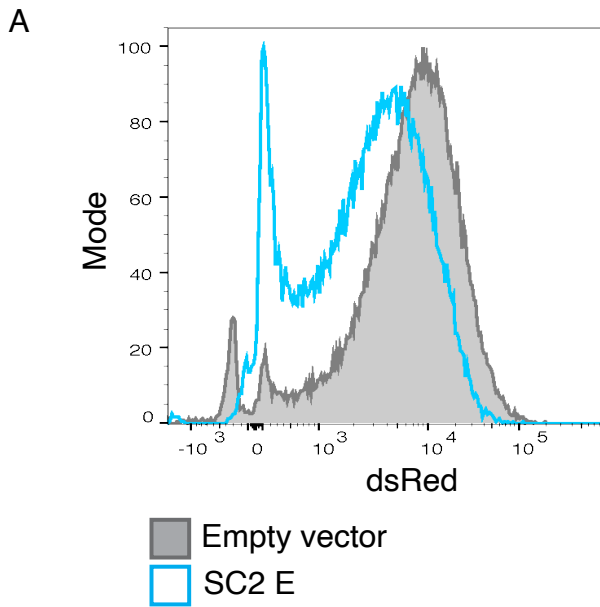
21

A

B

C

D

Figure 2.7: **SARS-CoV-2 Envelope leads to decreased ERAAP levels.** A. HEK293T cells were co-transfected with ERAAP dsRed and SC2 E (blue histogram), or empty vector control (grey filled histogram) and ERAAP dsRed levels were measured by flow cytometry. Histogram shows ERAAP dsRed levels within transfected cells 24 h post-transfection. B. The geometric mean fluorescence intensity (gMFI) for dsRed was obtained from HEK293T co-transfected with ERAAP dsRed and SC2 E, or empty vector as in A. Graphs shows the percent dsRed gMFI 24 h and 48 h after transfection with SC2 E relative to empty vector across 3 independent experiments. Cells that were co-transfected with empty vector were assumed to represent 100% ERAAP dsRed levels and are shown as a control. Data represents mean± SD. Unpaired One-way ANOVA assuming a Gaussian distribution and Tukey's multiple comparisons test was performed. *** p value < 0.001, ns=not significant. C. Representative blot showing ERAAP levels in HEK293T co-transfected with ERAAP 3XFlag and SC2 E, SC2 S, or empty vector control. WCL collected 36 h post transfection. GAPDH is shown as a loading control. D. From blots as that shown in C, the band intensity of ERAAP 3XFlag and GAPDH was determined using Image J. The relative ERAAP levels for each condition was obtained after normalizing to respective GAPDH levels. Graph shows the percent ERAAP 3XFlag levels in HEK293T transfected with SC2 E or an unrelated protein (ex. SC2 S). Cells that were co-transfected with ERAAP 3XFlag and empty vector were assumed to represented 100% ERAAP levels and are shown as a control. Data represents mean ± SD from 5 independent experiments for cells co-transfected with vector or SC2 E and from 3 experiments for unrelated protein. Unpaired One-way ANOVA assuming a Gaussian distribution with Tukey's multiple comparisons test was performed. *** p value < 0.001, **** p value < 0.0001.
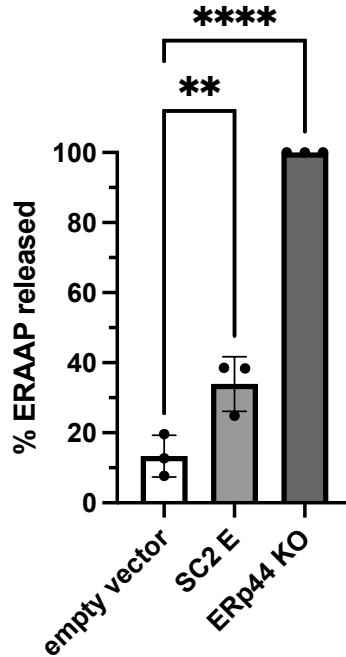
Figure 2.8: **ERAAP is secreted from cells expressing SARS-CoV-2 Envelope.** LAP assay was performed on the supernatants of NIH 3T3 ERAAP dsRed cells transfected with empty vector or SC2 E. Background activity detected in the supernatant of untransfected NIH 3T3 ERAAP dsRed cells was subtracted from all conditions. LAP activity from the supernatant of NIH 3T3 ERAAP dsRed ERp44 KO cells was measured and assumed to represent 100% ERAAP release. Graph shows the percent of ERAAP released for each condition. Data represents mean $\pm$ SD from 3 independent experiments. Unpaired One-way ANOVA assuming a Gaussian distribution with Dunnett's posttest was performed. ** p value < 0.01, **** p value < 0.0001. Cell line used in this experiment was generated by Dan Tran.
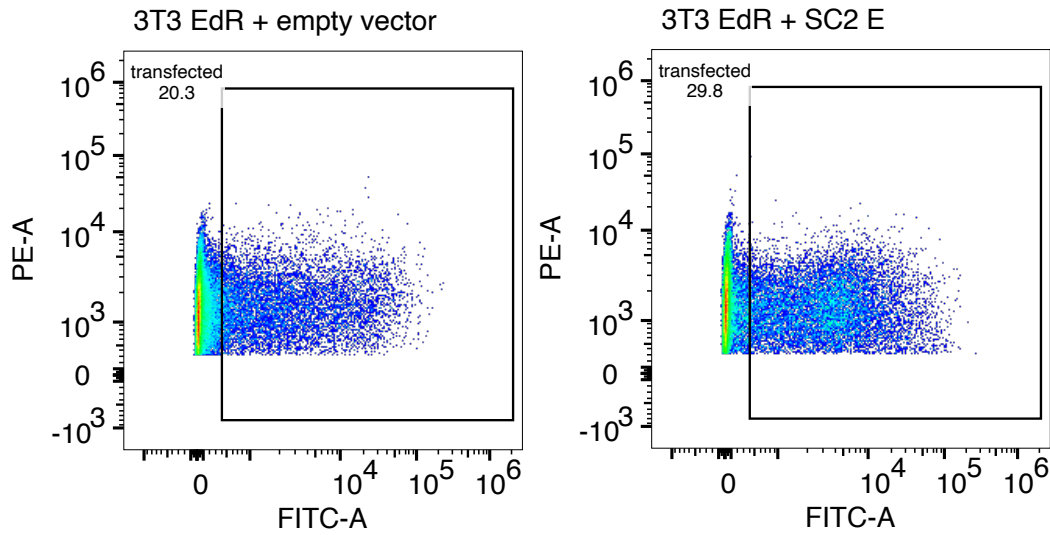
Figure 2.9 **Transfection efficiency of NIH 3T3 ERAAP dsRed cells transfected with SARS-CoV-2 Envelope.** NIH 3T3 ERAAP dsRed cells were transfected with empty vector or SC2 E. The supernatant was collected for LAP assay (Figure 2.8) and the cells were used to measure transfection efficiency by flow cytometry 48 h post-transfection. Flow plots show the percent of cells that are expressing SC2 E or empty vector (GFP reporter detected with FITC channel) within cells that are expressing the ERAAP dsRed construct (dsRed detected with PE channel). Cell line used in this experiment was generated by Dan Tran.

2.4. Conclusions

Using a CRISPR KO screen, we identified ERp44 as the main host factor regulating ERAAP retention in cells. ERp44 KO cells showed decreased intracellular ERAAP levels and increased secretion of ERAAP into the extracellular environment. ERp44-mediated retention of ERAAP is in part regulated by pH. Here we report that pH disruption by SARS-CoV-2 E interferes with ERAAP retention in the ER and leads to its secretion. The increase of Golgi pH by E is an essential part of the SARS-CoV-2 viral life cycle as it protects the S protein from being inadequately processed by proteases residing in the Golgi[26,89].

To avoid detection by CD8^{+} T-cells, viruses have evolved a myriad of immune evasion mechanisms aimed at preventing the presentation of antigenic peptides[64,82]. Interfering with ERAAP likely represents another one of these strategies, as illustrated by HCMV and likely MCMV[83–85]. Furthermore, a recent study by Stamatakis, et al., showed that ERAP generates potentially immunogenic SARS-CoV-2 S-derived peptides predicted to bind MHC[91]. Here we show that SARS-CoV-2 E leads to a decrease in ERAP intracellular concentration. This suggests that targeting the Golgi by SARS-CoV-2 could preserve the integrity of the viral fusion protein S and dampen the generation of virally-derived antigenic peptides through the loss of ERAP. Given the central role of ERAP in modulating T-cell responses, other viruses beyond HCMV, MCMV, and SARS-CoV-2 may have also evolved to disrupt ERAP as part of their immune evasion strategies.

Fortunately, viral immune evasion does not go unchallenged. Cells and the immune system have evolved mechanisms to sense and respond to virally-mediated disturbances. In mice, ERAAP dysfunction is sensed by QFL T-cells. MCMV-induced ERAAP loss results in the presentation of the self-peptide FL9 in the MHC-I molecule Qa1b, the activating ligand of QFL T-cells. In infected mice, QFL T-cells are activated, produce inflammatory cytokines, and can kill cells experiencing ERAAP loss[85]. This exciting observation suggests that ERAAP dysregulation during infection has the potential to be sensed by the immune system. The existence of QFL-like T-cells in humans has yet to be described, but it is tempting to speculate that if a similar immune response exists, it could aid in controlling SARS-CoV-2 infection.

In addition to the loss of intracellular ERAP, we showed that ERAP is secreted from cells expressing SARS-CoV-2 E. Secreted ERAP has been implicated in blood pressure regulation which might have consequences for SARS-CoV-2 infection. ERAP's potential to modulate the renin-angiotensin-aldosterone system (RAAS), which controls blood pressure, comes from its ability to cleave Angiotensin II (Ang II) into Ang III and Ang IV[92]. Ang II exerts its effects on multiple organs that work in concert to raise blood pressure[93]. To maintain normotension, Ang II levels are carefully regulated. Ang II is cleaved into other angiotensin products that can activate parallel pathways which have the opposite effect of lowering blood pressure[94]. Ang II is usually cleaved by angiotensin-converting enzyme 2 (ACE2). ACE2 has gathered much attention as it is the primary receptor SARS-CoV-2 uses to enter cells[95,96]. Upon interaction of SARS-CoV-2 S with ACE2, the virus is internalized causing a temporary depletion of ACE2 at the cell surface,

which can result in local increases of Ang II levels[97,98]. Dysregulated RAAS is thought to contribute to the clinical manifestations of COVID-19[99–102]. As recently proposed by D'Amico et al., secreted ERAP could help alleviate some of these effects by lowering the levels of Ang II[101]. Our findings provide the first indication that ERAP can be secreted from SARS-CoV-2 infected cells opening the possibility that ERAP might regulate RAAS during infection. Future studies are needed to address the specific contribution of ERAP as a potential protective factor during SARS-CoV-2 infection. Interestingly, some ERAP polymorphisms predicted to result in lower ERAP activity or loss of function have been linked to hypertension and blood pressure progression[101]. It is possible that patients with dysfunctional ERAP could be susceptible to more detrimental COVID-19 outcomes because of an inability to dampen Ang II levels. One described ERAP polymorphism, A1533G, results in reduced activity and inability to convert Ang II into its cleavage products[103]. Given these observations, it is certain that the role of ERAP in SARS-CoV-2 infection merits more investigation due to the potential of ERAP to protect or contribute to COVID-19 pathology.

As shown here by us and others, ERAAP localization and retention are regulated by the chaperone ERp44[87]. ERp44 is a member of the protein disulfide isomerase family that cycles between the ER, ERGIC, and cis-Golgi. ERp44 interacts with client proteins, such as ERAP, that lack ER retention motifs (i.e. KDEL) and retrieves them from the Golgi back into the ER. Importantly, ERp44's function is regulated by pH. In the neutral environment of the ER, ERp44 adopts a close conformation in which its carboxyl (C-) terminal tail occludes the client binding site. In the acidic environment of the ERGIC and cis-Golgi, ERp44 undergoes conformational changes that liberate its C-terminal tail and make its binding pocket accessible for client binding[86]. The C-terminus of ERp44 contains an RDEL sequence that facilitates the transport of the ERp44-client complex from the Golgi to the ER via KDEL receptors[90]. Similar to what we reported here, increasing the Golgi pH by silencing the Golgi pH regulator (GPHR) results in a decreased ability of ERp44 to bind its clients, and secretion of clients to the extracellular space[88]. In addition to ERAP, ERp44 regulates other clients, including Ero1β, Prx4, and SUMF1[90,104,105]. Secretion of these clients has been reported in cases where interactions with ERp44 are perturbed. We thus speculate that these may also be secreted by SARS-CoV-2 E-expressing cells. Whether these other clients have extracellular functions, and whether their secretion is physiologically relevant remains to be explored.

The observation that pH dysregulation leads to ERAAP loss potentially extends beyond SARS-CoV-2. The E protein belongs to a larger family of virally encoded ion channel-like proteins collectively known as viroporins. Due to their ability to change membrane permeability, viroporins induce a range of physiological changes in the cell. They are encoded by viruses across many different families[4,20] including some that are clinically relevant like IAV, HIV, and HCV. Of all viroporins, the best studied is IAV M2. M2 is a multifunctional pH-regulated ion channel and similar to SARS-CoV-2 E, M2 localizes to the Golgi membranes where it neutralizes the pH of this organelle[23–26]. For M2, modulating Golgi pH helps protect HA from preemptively adopting the low pH conformation needed for fusion[25]. The p7 protein from HCV has also been shown to disrupt H$^+$ gradients and increase intracellular pH[27]. It would be interesting to test whether infection with viruses like IAV and HCV could also result in ERAP loss and secretion.

Given that ERAP's primary function is peptide trimming in the ER, it is interesting that this protein lacks an ER retention signal and instead relies on ERp44 for its proper localization and function. This reliance on ERp44 makes ERAP susceptible to different modes of regulation. Indeed, in addition to pH perturbation, ERp44 function is abrogated by disruption of the oxidoreductive state in the ER/Golgi[87,90], changes in the Zn^{2+} gradient of the secretory pathway[106], as well as altered trafficking between the Golgi and the ER. This reliance on pH, redox, or Zn^{2+} homeostasis for ERp44 function thus suggests that perturbation of these elements, whether mediated by a disease state or an infection, should lead to loss of ERAP. Since the loss of ERAP is associated with the presentation of an alternative immunogenic peptide repertoire on MHC-I molecules, it is expected that perturbation of these pathways would lead to the elimination of the affected cells by the immune system. Notably, because viruses rely on co-opting the secretory pathway to produce viral proteins and the assembly of virions, one can reason that it will be difficult for viruses to evade activating pathways that sense perturbations in these compartments. Taken together, we propose that ERAP could serve as a sensor of intracellular disturbances and a link between cellular sensing and activation of the immune system.

2.5. Materials and Methods

Cell lines

HEK293T, HeLa cells, and Phoenix cells were obtained from the UC Berkeley Cell Culture Facility. NIH 3T3, BJAB, and MC57G cells were purchased from ATCC. Except for BJAB, all cells were cultured in DMEM (Gibco, 11995073) containing 10% FBS (VWR, 89510-186) and 1% Pen Strep (Gibco, 15140-122). BJAB cells were cultured in RPMI (Gibco, 11875) containing 10% FBS and 1% Pen Strep. Cells were cultured at 37 °C in 5% CO_2.

Generation of ERAAP-dsRed cell lines

To generate stable cell lines expressing ERAAP-dsRed, cells were transduced with retrovirus produced in Phoenix cells. Briefly, Phoenix cells were seeded at 500,000 cells/well in a 6-well plate. 24 hours later, cells were transfected with 2 ug of pQCXIN ERAAP-dsRed using Fugene HD transfection reagent (Promega, E2311) following the manufacturer's instructions. 48 hours post-transfection, the supernatant was harvested, filtered through a 0.45 μM filter, and added to BJAB or NIH 3T3 target cells.

BJAB transduced to express ERAAP-dsRed were selected with 1 mg/mL neomycin (G418; Corning, 61234RF). After selection, cells were sorted based on high dsRED expression by FACS. Sorted cells were subcloned to identify a clonal population of cells with uniform high expression of ERAAP-dsRed (Clone B2 and D4). HEK293T cells were used to produce lentivirus encoding Cas9 (lentiCas9-Blast, Addgene #52962, gift from Feng Zhang). BJAB ERAAP-dsRed cells were seeded at 1X10^6 cells/well in a 12-well plate and spin-infected with Cas9 expressing lentivirus in the presence of 4ug/mL polybrene (Santa Cruz Biotechnology, sc-134220) by centrifugation at 1,000 g for 2 h at 33 °C. 24 h after transduction, the selection was started by culturing cells in media containing 5 ug/mL blasticidin (AG Scientific, B-1247). The selection was continued for 7 days to allow non-transduced cells to die and be removed from the population. BJAB ERAAP-dsRed expressing Cas9 (Clone B2) was selected to perform the genome-wide CRISPR screen.

To generate NIH 3T3 cells expressing ERAAP-dsRed, 200,000 cells/well were seeded in a 6-well plate and supernatant containing retrovirus encoding ERAAP dsRed was added. Cells were spinfected with polybrene at 1,200 rpm for 2 hours. Media was replaced and cells were left to recover overnight. The next day, the selection was started by incubating the transduced cells with media containing 1 mg /mL neomycin (G418). Cells were selected for 10 days and dsRed expression was evaluated by flow cytometry. To isolate a homogenous population of cells expressing ERAAP-dsRed, cells were subcloned. Cell clones were screened by flow cytometry to confirm uniform dsRed expression. Single-cell clone F3 was identified and was used to generate ERp44 KO cells in this background.

Genome-wide CRISPR KO screen

6.0 X 10^6 BJAB clone B2 cells expressing both Cas9 and ERAAP dsRed were transduced with lentivirus of human GeCKO v2 library (Addgene, #1000000049, gift from Feng Zhang) at an multiplicity of infection (MOI) of 0.4 using spin-infection (1,000 g for 2 h at 33 °C). After selection with 3 ug/mL puromycin for 7 days, cells were sorted by flow cytometry based on ERAAP dsRed expression levels. Cells with the top and bottom 10-15% of ERAAP dsRed expression were sorted and collected by FACS for each GeCKO sublibrary (A and B). Genomic DNA was extracted from sorted cells to sequence enriched guide RNA (sgRNA) sequences in each population. Using a two-step nested PCR with KAPA HiFi HotStart ReadyMixPCR Kit (Kapa Biosystems), sgRNA expression cassettes were amplified. PCR products were gel-purified using a QIAquick Gel Purification kit (Qiagen) and sequenced on an Illumina NextSeq 500 using custom sequencing primers. Fastq files were analyzed using the Model-based Analysis of Genome-wide CRISPR/Cas9 Knockout (MaGeCK) method[107].

Generation of ERp44 KO cell lines

To generate ERp44 KO cells, cells were first transduced to express Cas9. Generation of BJAB ERAAP-dsRed expressing Cas9 is described above. The same procedure was followed to generate Cas9 expressing NIH 3T3 and MC57G cells.

Guide RNAs targeting ERp44 were cloned into the lentiviral vector pLKO.1 to generate a pLKO.1-ERp44sgRNA lentiviral vector. Sequences for the sgRNAs used are included below.

gRNA	Sequence
ERp44 Mouse sgRNA F1	CACCGTGTAATCTACAAACCACCCG
ERp44 Mouse sgRNA R1	AAACCGGGTGGTTTGTAGATTACAC
ERp44 Mouse sgRNA F2	CACCGAATGTTATTTCTCGGACAAG
ERp44 Mouse sgRNA R2	AAACCTTGTCCGAGAAATAACATTC
ERP44 Human sguide F1	CACCGGTGCTGATCACAATCAACTC
ERP44 Human sguide R1	AAACGAGTTGATTGTGATCAGCACC
ERP44 Human sguide F2	CACCGCCTCACTCACCAGGAGCAGA
ERP44 Human sguide R2	AAACTCTGCTCCTGGTGAGTGAGGC

To generate ERp44 KO cell lines for BJAB ERAAP-dsRed (clone B2), NIH 3T3 and MC57G, HEK293T cells were plated at 500,000 cells/well in a 6-well plate. After 24 hours, cells were transfected with 250 ng VSVG, 1,250 ng of psPAX2, and 1,250 ng of pLKO.1-ERp44sgRNA using TransIT-LT1 transfection reagent (Fisher Scientific, MIR2300) following manufacturer's instructions. After 48 hours, supernatant from transfected HEK293T cells was collected and filtered using a 0.45uM filter. Lentivirus with polybrene was added to target cells plated in a 6-well plate. Cells were spinfected for 2 hours after which fresh media was added to the cells. 24 h later, cells were put into puromycin supplemented media to select for cells expressing ERp44

guide RNA (BJAB ERAAP-dsRed and NIH 3T3-2 ug/mL puromycin, MC57G-4 ug/mL puromycin). After 7 days, KO efficiency was assessed by western blot.

To generate ERP44 KO cells in the NIH 3T3 ERAAP-dsRed background, cells were first transduced to express Cas9. HEK293T cells were transfected with 500 ng VSVG, 500 ng of pRRE, 500 ng of pRev, and 1000 ng of pFUGW-Cas9. 48 h after transfection, lentivirus was harvested and NIH 3T3 ERAAP-dsRed cells (Clone F3) were spinfected as described above. Cells were selected with 5 µg/mL blasticidin for 9 days. The resulting Cas9-expressing NIH 3T3 ERAAP were used to generate ERP44 KO cells. ERp44 mouse sgRNA F1 and R1 were cloned into hLKO to generate hLKO-ERp44sgRNA. NIH 3T3 ERAAP-dsRed cells were transduced with lentivirus encoding ERp44 sgRNA and selected for 9 days in the presence of 200 µg/mL Hygromycin. ERp44 KO was confirmed by western blot.

Generation of ERAAP KO cells

BJAB ERAAP-dsRed, NIH 3T3, and MC57G expressing Cas9 were transfected with gsRNA targeting ERAAP as described above. gRNAs used:

ERAAP sgRNA F1: CACCGCAGTGGATCAAATTTAACGT
ERAAP sgRNA R1: AAACACGTTAAATTTGATCCACTGC

ERAAP KO splenocytes used for western blot were obtained from ERAAP KO mice that have been previously described (Hammer et al., 2006; Nagarajan et al., 2016).

Endo H assay

Whole cell lysate (WCL) for BJAB ERAAP-dsRed clones B2 and D4 was made using RIPA lysis buffer (150 mM NaCl, 1% Triton X-100, 5% Na Deoxycholate, 1% SDS, 50 mM Tris pH 8 in water) with Protease inhibitors (Roche, 11836170001). WCL lysate was incubated on ice for 30 minutes and centrifuged at max speed for 10 minutes to remove debris. Cleared lysate was transferred to a new tube and anti-ERAAP L1 antibody (1:200 dilution) was added. Samples were incubated rotating overnight at 4 °C. The next day, ERAAP was immunoprecipitated by adding 40 ul of Protein A Dynabeads (Invitrogen, 10001D) to each sample and incubating an additional 2 hr. Using a magnet, beads containing ERAPP were captured. Beads were washed four times with 50 mM Tris, 150 mM NaCl in water. Endo H assay was performed following manufacturer's instructions (New England Biolabs, P0702S). Following addition of Glycoprotein Denaturing Buffer, each sample was aliquoted into two tubes. 1 ul of EndoH (Endo H +) or 1 ul of water (Endo H -) was then added to each tube. Samples were incubated for 1 h at 37 °C. ERAAP's glycosylation state was assessed by western blot. Membrane was probed using anti-ERAAP L1 antibody (1:000 dilution). Anti-ERAAP L1 was produced in the Shastri lab.

ERAAP western blot on cells co-transfected with ERAAP 3XFlag and SARS-CoV-2 E

HEK293T cells were seeded at 1X10^6 cells/well in a 6-well plate. The next day, cells were transfected with 1 ug of plasmid encoding ERAAP 3XFlag (pCDNA3.1 background) and 1 ug of control plasmid (pIRES-GFP), pIRES-GFP SARS-CoV-2 E, or pIRES-GFP SARS-CoV-2 Spike using Fugene HD following manufacturer's instructions. WCL was collected 36 hours post transfection. Briefly, cells were washed once with PBS (Gibco, 10010023) and detached using trypsin (Gibco, 25300062). Cells were centrifuged at 1,600 rpm for 8 min. Supernatant was carefully removed and cell pellet was resuspended in RIPA lysis buffer with Protease inhibitor. WCL was incubated with 1% Benzonase (Sigma, 1014-25KU) for 15 min at 37 °C. Cleared lysates were collected by centrifuging Benzonase-treated samples for 10 min at 15,000 rpm (4 °C) to pellet remaining genomic DNA.

For western blot, protein concentration was determined using Pierce BCA Protein Assay Kit (Thermo Scientific, 23225) following manufacturer's instructions. A total of 50 ug of WCL was combined with 4X Laemelli Sample Buffer (BioRad, 1610747) to a final concentration of 1X sample buffer, boiled for 5 min at 100 °C, and loaded into 4-15% Mini-Protean TGX gels (Biorad, 4561084). Gel was run for 1 hr at 120V after which proteins were transferred (1.3 A, 25V, 10 min) into PVDF membranes and blocked for 1 hr at room temperature with 3% bovine serum albumin (BSA) buffer (3% bovine serum albumin, 1 % Triton X-100, 0.5% Tween-20 in PBS). Primary and secondary antibodies were diluted in 3% BSA buffer. Membranes were incubated with the following antibodies: anti-FLAG M2 (Sigma, F1804; 1:1000 dilution), anti-GAPDH 0411 (Santa Cruz Biotechnology, sc-47724; 1:1000 dilution). Primary antibody incubation was done overnight at 4 °C. The next day, the membranes were washed 3 times with PBS for 5 min each and incubated with secondary antibody for 1 hr at room temperature. Secondary antibody used was IRDye 680RD Donkey anti-Mouse IgG (Licor, 926-68072; 1:10000 dilution). Imaging was done using a ChemiDoc MP imager (Biorad). Band intensity analyzed using Image J 1.52q.

ERAAP western blot on ERp44 KO cell lines

ERp44 KO and WT cell lines (BJAB ERAAP dsRed, NIH 3T3, and MC57G) were lysed in lysis buffer containing 25 mM Tris-HCl (pH 7.6), 150 mM NaCl, 0.1% SDS, 0.5% sodium deoxycholic, and protease inhibitors (Roche) for 30 minutes on ice. Samples were then centrifuged at 20,000xg for 10 min at 4°C to clarify lysate. Lysates were separated by SDS-PAGE and western blot was performed. Membranes were incubated with the following antibodies: anti-ERAAP L1 (1:1000), anti-ERp44 (Invitrogen, #PA5-28484; 1:1000 dilution), anti-GAPDH (Abcam, ab8245; 1:5000 dilution). Rabbit anti-ERAAP L1 was produced in the Shastri lab.

Golgi pH measurement

pH reporter assay was done as described[26]. The pHluorin plasmid was kindly provided by Dr. Carolyn Machamer. Briefly, HeLa cells were seeded at 1X10^6 cells/well in a 6-well plate. The next day, cells were transfected with 2 ug of pHluorin TGN38 alone for generating a standard curve or with 1 ug each of pHluorin TGN38 and pIRES-RFP SARS-CoV-2 E, or pIRES-RFP IAV M2.

18 hours post transfection, media was removed, and cells were washed once with serum free (SF) DMEM. Cells were then incubated for 1 hr at 37 °C with 100 ug/mL cycloheximide (Sigma-Aldrich, C4859) in SF DMEM. Cycloheximide was removed and cells were washed once with PBS, detached using trypsin, and neutralized with ice-cold SF DMEM. Cells were pelleted by spinning 10 min at 1,600 rpm and then washed twice with SF-DMEM. To generate a pH standard curve, cells transfected with pHluorin were resuspended in Na-Ringer buffer (140 mM KCl, 2 mM CaCl$_2$, 1 mM MgSO$_4$, 1.5 mM K$_2$HPO$_4$, 10 mM Glucose, 10 mM 2-(N-Morpholino)ethanesulforic acid sodium salt,10 mM HEPES) containing 10 uM monensin (Research Products International, M92100-1.0) and 10 uM nigericin (Cayman Chemical, 11437-5). Cells co-transfected with pHluorin and viral proteins were resuspended in Na-Ringer buffer. Samples were analyzed in the LSR Fortessa Celeste or LSR Fortessa X20 cytometer (BD Biosciences). pH reporter was excited at 405 nm and 408 nm and the emitted fluorescence recorded on FACS Diva software v8.0.1. Data was analyzed in Flow Jo (v10) and the pHluorin emission ratio for each sample was obtained by creating a ratio between the fluorescence emitted after excitation at 405 nm and 488 nm (405 nm/488 nm). The geometric mean of the pHluorin emission ratio was used to obtain a pH value for each sample. The emission ratio of samples resuspended in buffers of known pH was used to generate a standard curve and the formula obtained was used to calculate the luminal Golgi pH of the experimental samples.

ERAAP dsRed reporter assay

HEK293T cells were seeded at 1X10^6 cells/well in a 6-well plate. The next day, cells were transfected with 1.3 ug of plasmid encoding ERAAP-dsRed (pQCXIP background) and 700 ng of pIRES-GFP, pIRES-GFP SARS-CoV-2 E, or pIRES-GFP SARS-CoV-2 Spike using Fugene HD following manufacturer's instructions. Cells were harvested for flow cytometry analysis at 24 h and 48 h post-transfection. Briefly, cells were washed with PBS, detached using typsin, and neutralized with DMEM 10% FBS. Cells were centrifuged at 1,600 rpm for 8 min to pellet. Cell pellet was resuspended in flow buffer (3% FBS, 1 mM EDTA in PBS). Cells were washed 2-3 times with flow buffer. Samples were incubated 10 min on ice with viability dye (Invitrogen, 65-0865-14) after which cells were pelleted and resuspended in flow buffer for analysis.

BJAB, BJAB ERAAP-dsRed, and BJAB ERAAP-dsRed ERp44 KO cells were harvested by centrifugation at 1,600 rpm for 8 min. Cell pellets were resuspended in flow buffer (3% FBS, 1 mM EDTA in PBS) and washed 2-3 times before resuspending for analysis.

NIH 3T3, NIH 3T3 ERAAP-dsRed, and NIH 3T3 ERAAP-dsRed ERp44 KO cells were washed with PBS, detached using typsin, and neutralized with DMEM 10% FBS. Cells were centrifuged at 1,600 rpm for 8 min to pellet. Cell pellets were resuspended in flow buffer (3% FBS, 1 mM EDTA in PBS). After 2-3 washes with flow buffer, cells were resuspended in flow buffer for analysis.

Samples were analyzed using the LSR Fortessa Celeste or LSR Fortessa X20 cytometer (BD Biosciences) and data recorded on FACS Diva software v8.0.1. Data was analyzed in Flow Jo (v10).

ERAAP secretion assay

To evaluate ERAAP secretion from BJAB ERAAP-dsRed ERp44 KO cells, ERAAP was first immunoprecipitated from the supernatant. Cells were seeded at 100,000 cells/well. After 36 h, supernatant was harvested and centrifuged at 1,500 rpm for 5 min to remove cells. Cleared supernatant was incubated with anti-ERAAP L1 antibody (1:50 dilution) for 1 h rotating at 4 °C. ERAAP was immunoprecipitated by adding 50 ul of Protein A Dynabeads (Invitrogen, 10001D) to each sample and incubating for 1 h rotating at 4 °C. Using a magnet, beads containing ERAPP were isolated. Beads were washed four times with PBS and resuspended in 75 uL of PBS. 50 uL of resuspended beads was used for LAP assay.

To measure ERAAP secretion from cells expressing SARS-CoV-2 E, NIH 3T3 ERAAP-dsRed cells were seeded at 200,000 cells/well in a 12-well plate. The next day, cells were transfected with 1 ug of pIRES-GFP (empty vector) or pIRES-GFP SARS-CoV-2 E using Fugene HD following manufacturer's instructions. Approximately 18 h post transfection, the media was changed to DMEM without phenol red (Gibco, A18967-01). This media was supplemented with 10% FBS, 1% Pen Strep, 1 mM Sodium Pyruvate (Gibco, 11360-070) and 2 mm L-Glutamine (Gibco, 25030-081) to match previous culturing conditions. 48 h after transfection, supernatant was collected. Cell debris was removed by centrifugation at 1,500 rpm for 5 min. Cleared supernatant was moved to a new tube. 50 uL of supernatant was used for LAP assay.

LAP assay was performed by incubating 50 uL of beads containing ERAAP (for BJAB) or 50 uL of supernatant (for NIH 3T3) with 100 ul of 2 mg/mL (in 50 mM Tris, pH 7.6) leucine p-nitroanilide (LpNA; Sigma, L9125). Samples were incubated at 37 °. Cleavage of the peptide substrate results in a colorimetric change that was detected at OD 410 nm. LAP activity was assessed 8 h after addition of the substrate for BJAB cell lines and 19-20 h for NIH 3T3 cell lines.

Statistical Analysis

Unpaired T-test or Unpaired One-way ANOVA with multiple comparisons analysis was performed in Graph Pad PRISM version 9.4.1 for MacOS. Compiled data is shown as mean± SD.

III

Chapter III: Attempts towards understanding MCMV M18's function in cells

3.1 Introduction

MCMV M18

HDACs play essential roles in regulating viral gene expression during herpesvirus infection and latency. Consequently, viruses have evolved to encode viral proteins that modulate the activity of these enzymes. Our lab discovered that the M18 protein from MCMV functions as an HDAC inhibitor[108]. This work stemmed from the study of Natural Killer (NK) cell recognition of MCMV-infected cells. NK cells are innate lymphocytes that respond to cellular abnormalities resulting from infection or transformation and lead to the elimination of these cells[109]. It was found that MCMV-infected cells induce transcription of a family of stressed-induced NK cell ligands called Rae-1[110,111]. Rae-1 ligands are recognized by the activating receptor NKG2D on NK cells, which triggers NK-cell mediated killing of the target cells. These ligands are not expressed by healthy cells but are induced in stress conditions associated with cancer and infection[112,113]. This suggested that these ligands must be actively repressed in normal cells. Importantly, during infection, this transcriptional induction is antagonized by several viral proteins that prevent the presentation of these ligands at the cell surface, thus avoiding NK-cell mediated killing[114,115].

Work in our lab identified M18 as both necessary and sufficient for Rae-1 induction during MCMV infection[108]. Transfection of m18 sensitized cells to NK-cell mediated killing in an NKG2D dependent manner. Further characterization revealed that the Rae-1 promoter is normally repressed by the action of HDAC3 and the Sp3 transcription factor. M18 alleviates this repression by preventing activation of HDAC3 by the cellular kinase CK2[116]. In this way, M18 functions as a HDAC inhibitor. Indeed, treatment of cells with chemical HDAC inhibitors induces expression of Rae-1 ligands[108]. Furthermore, transfection of cells with the virally encoded HDAC inhibitors ICP0 from HSV-1 and IE1 from HCMV also resulted in Rae-1 ligand upregulation.

Infection of mice with a virus lacking the m18 open reading frame (ORF), Δm18 MCMV, revealed that this protein is dispensable for growth in tissue culture and in the spleen, lung, and livers of infected mice. However, M18 was required for efficient infection of the salivary glands[117]. Up to 1,000-fold less Δm18 MCMV virus was recovered from this organ in comparison to WT MCMV. Importantly, the salivary glands represent an organ where MCMV can be detected for weeks after initial infection[118]. This organ facilitates transmission of the virus[119] highlighting its importance as a reservoir. The mechanism by which M18 allows for infection of the salivary glands is not known.

Further characterization of M18 revealed that two polypeptides are produced from the m18 ORF[117]. Specifically, an alternative splicing event within m18 gives rise to two distinct proteins, a 180 kDa isoform named M18 L and a smaller ~70 kDa isoform named M18S. Addition of an N-terminal FLAG tag to m18 results in the detection of both protein products. In contrast, an m18 construct containing a C-terminal HA tag yielded a single band corresponding to M18L. This suggested that M18L and M18S share an N-terminus but have unique C-termini. Transcripts corresponding to both forms of m18 were identified in cells transfected with m18. Using a

combination of mutagenesis and sequencing tools, the splicing donor and acceptor sites that drive the production of m18S were identified. It was found that m18S results from a splicing event between nucleotides 1206 and 1367. This splicing event results in a frameshift and use of an alternative stop codon at position 1447 within m18.

Additional work suggested that M18L and M18S are functionally distinct. Cells transfected with m18 1365G, which encodes for M18L, showed induction of Rae-1 ligands to similar levels as observed with WT M18. No Rae-1 induction was observed in cells expressing M18S[117]. This led us to hypothesize that M18L and M18S might have unique functions.

Project rationale

This project aimed to further characterize the function of M18 in cells. Because Rae-1 induction would sensitize cells to killing by NK cells and the virus encodes proteins that actively counteract this response, it is unlikely that the function of M18 is to upregulate these ligands. Instead, this is the unintended result of HDAC inhibition. As HDACs could potentially impact different aspects of herpesvirus infection, we became interested in deciphering the specific role of M18 during MCMV infection. To gain insights into the function of M18, we assessed if M18L and M18S are differently produced or localized during infection. Furthermore, because inhibition of HDACs can alter gene expression, we evaluated the transcriptional changes caused by M18 during infection using RNAseq.

3.2 Results

M18 exists as two distinct proteins during MCMV infection

The initial discovery and characterization of M18L and M18S was made in cells transfected with m18. However, the presence of these two M18 isoforms had not been evaluated during infection. It is possible that the presence of other viral proteins and/or the cellular response to infection could result in differential regulation of M18 in infected cells versus transfection. First, we wanted to evaluate if M18L and M18S are produced during infection. Because antibodies against M18 do not exist, we decided to tag M18 to allow for detection of this protein endogenously. I introduced an N-terminus 3XFlag to m18 using homologous recombination within the bacterial artificial chromosome (BAC) containing the MCMV genome. Introduction of this tag did not interfere with viral production.

To evaluate M18 expression during infection, NIH 3T3 cells were infected with 3XFlag m18 MCMV at MOI 5 for 24 h. Next, WCL was collected, and protein levels were evaluated by western blot. Infection with 3XFlag m18 MCMV resulted in the production of both forms of M18, as evidenced by the presence of a high molecular weight band at ~180 kDa corresponding to M18L and a smaller product at ~70 kDa corresponding to M18S (Figure 3.1A). No background signal was obtained from cells infected with untagged WT MCMV. The sizes of the two M18

protein products are consistent with those obtained in cells transfected with a 3XF m18 construct.

Next, we assessed the kinetics of M18L versus M18S expression during infection. Cells were infected with 3XFlag m18 MCMV, and WCL was collected at 2, 4-, 6-, 12-, and 24-hours post-infection (hpi). M18 expression was assessed by western blot. Our results show that M18 was present as early as 4 hpi, but only the short form of M18 (~70 kDa) was detected at this timepoint (Figure 3.1B). At 6 hpi, a high molecular weight band (~180 kDa) corresponding to M18L was observed. Taken together, our results demonstrate that M18 exists as two distinct proteins during MCMV infection. These results are in accordance with our previous observations done using a transfection system.

Since we successfully tagged endogenous m18 in the context of the MCMV genome, we next wanted to generate mutant viruses that could only produce the long or short form of M18, respectively. We aimed to use the 3XFlag m18 MCMV, 3XFlag m18 L MCMV, and 3XFlag m18 S MCMV viruses to assess the functions of both forms of M18 during infection in cells and mice. Asha Pappajohn, my undergraduate mentee, performed BAC mutagenesis to introduce the splice acceptor mutation (1365 A-> G) into m18, which should generate a virus that can only produce m18L. In addition, she substituted m18 with the m18S sequence in the BAC. She successfully generated the BAC constructs encoding m18L and m18S, which were confirmed by sequencing. However, despite numerous attempts, we could not produce virus in high titers out of these BAC constructs. Virus is generated by transfecting NIH3T3 cells with the BAC DNA encoding the MCMV genome. Multiple vials of NIH3T3 cells were tested, but we could not get virus produced from these cells as measured by TCID50. Ultimately, these technical difficulties prevented us from generating the 3XFlag m18 L and 3XFlag m18 S MCMV and carrying out our planned experiments.

M18L and M18S show different localization patterns in cells

Because we could not obtain viruses encoding M18L and M18S, we decided to continue our experiments using a transfection system. To gain insights into the possible functions of M18S and how those might differ from M18L, we first decided to evaluate the cellular localization of these proteins. Previous data from the lab suggested that M18 was primordially localized to the nucleus[108]. However, these experiments were performed using a C-terminally tagged version of M18 fused to GFP or RFP, which would only allow the detection of M18L. Thus, we wanted to evaluate the localization of M18S and compare it with that of M18L. To this end, NIH3T3 cells were transfected with plasmid encoding 3XFlag m18, 3XFlag m18L, and 3XFlagm18S. The 3XFlag tag is localized in the C-terminus to allow the detection of both M18L and M18S in the WT m18 construct. We also decided to use the 3XFlag constructs since FLAG is relatively small compared to GFP and RFP. We wanted to decrease the possibility that fusion with the fluorescence proteins could affect M18's localization. 24 hpt, cells were fixed, and immunofluorescence (IFA) was performed. We visually assessed if cells showed an M18 signal in the cytoplasm, in the nucleus (overlapping with the DAPI signal), or in both the cytoplasm and the nucleus. Results are summarized in Figure 3.2A. Representative pictures are shown in Fig. 3.2B. For cells

transfected with WT m18 (pCMV 3XFlag m18 plasmid), we observed that most of the cells analyzed, ~62% (n=61), showed cytoplasmic staining exclusively. 32% of cells analyzed (n=29) showed M18 staining in both the nucleus and the cytoplasm and 9% showed nuclear only localization. For cells transfected with m18L, 78% (n=78) of cells showed cytoplasmic localization, ~18% (n=18) showed both nuclear and cytoplasmic localization, and ~3% (n=3) showed signal only in the nucleus. Interestingly, in cells expressing M18S, an almost equal fraction showed localization only in the cytoplasm (43%, n=34) and localization to the nucleus and cytoplasm (51%, n=40). The percent of cells that showed nuclear only localization (5%, n=4) remained low for cells transfected with m18S. Taken together, our data suggest that M18L and M18S have different localization patterns. M18L preferentially localized exclusively to the cytoplasm. In contrast, M18S showed more nuclear localization, as evidenced by a higher percentage of cells that showed both cytoplasmic and nuclear localization (51%) compared to cells expressing m18L (18%).

M18 induces expression of immune-related genes

As HDACs can regulate transcription as a result of their modification of histones and regulation of non-histone proteins[6], we would expect HDAC inhibition by M18 to result in changes to the transcriptome of the cell. To test this, we performed RNAseq on cells infected with WT MCMV compared to infection with a mutant virus lacking m18 (Δm18 MCMV). NIH 3T3 cells were infected at an MOI 10 to ensure most cells would be infected. RNA was collected at 18 hpi, and mRNAs enriched before library preparation and sequencing. Data analysis and visualization was done using Shiny Transcriptome Analysis Resource Tool (START)[120].

RNAseq analysis revealed a limited number of genes upregulated by M18, as evidenced by their enrichment in WT MCMV infected cells compared to Δm18 MCMV (Figure 3.4A). Gene Ontology and pathway analysis was performed to assess if genes regulated by M18 belong to any functional categories or pathways. Unexpectedly, we found that differentially expressed genes were enriched for immune pathways, in particular chemokine signaling and interferon response (Figure 3.4B). Specifically, many of these genes were induced during WT MCMV infection in an M18-dependent manner. The fold change in expression of these genes was modest (1.5-2-fold difference) but significant. Closer inspection of genes belonging to these networks revealed various members of the interferon-induced proteins with tetratricopeptide repeats (IFITs), a group of interferon-stimulated genes (ISGs), and chemokines (Figure 3.4C). Taken together, our results suggest that HDAC inhibition by M18 induces the expression of immune-related genes.
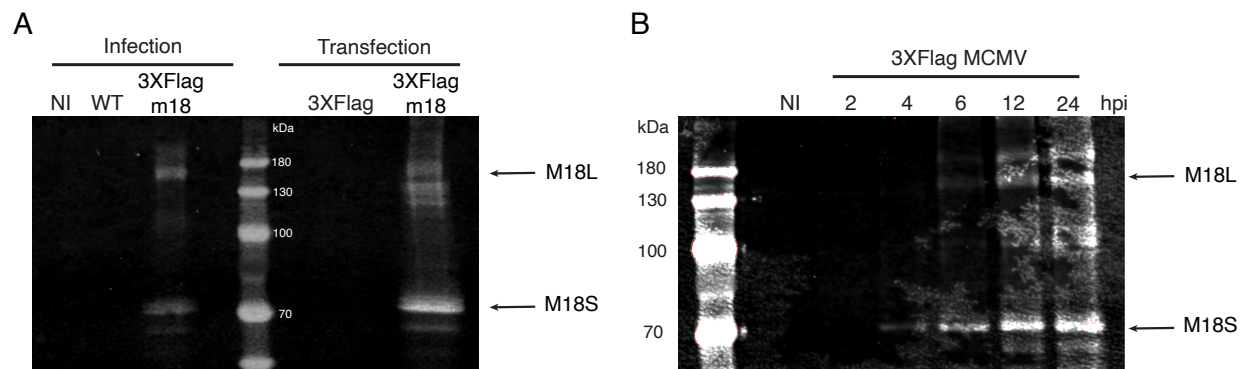
3.3 Figures

Figure 3.1: **M18 exists as two distinct proteins during MCMV infection.** A. NIH 3T3 cells were infected with WT MCMV or 3XFlag m18 MCMV or left uninfected (NI). As comparison, cells were transfected with a vector encoding 3XFlag m18 or empty vector as a control. WCL lysate was collected 24 h after infection or transfection. M18 levels were assessed by western blot. Shown is a representative blot after probing with anti-Flag antibody. M18L appears as a ~180 kDa molecular weight band (top arrow) while M18S appears as a ~70 kDa band (bottom arrow). B. NIH 3T3 cells were infected with 3XFlag m18 MCMV and WCL lysate was collected at 2, 4, 6, 12, and 24 hpi. Shown is a representative blot after probing with anti-Flag antibody. M18L is detected as a ~180 kDa molecular weight band (top arrow) while M18S appears as a ~70 kDa band (bottom arrow).

A

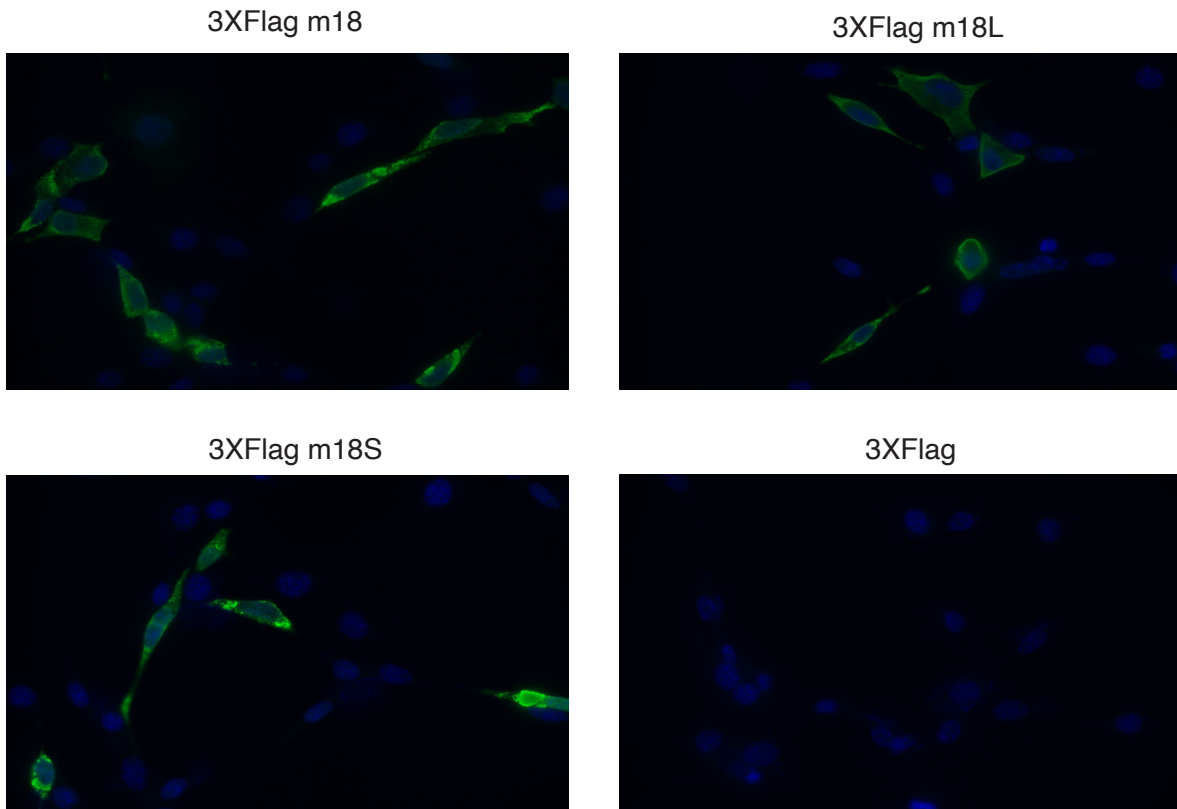| Condition	No. of cells analyzed	% nuclear only	% cytoplasmic only	% nuclear and cytoplasmic
m18	99	9.09	61.62	29.29
m18 L	101	2.97	78.22	17.82
m18 S	78	5.13	43.59	51.28

B

Figure 3.2: **M18L and M18S show different localization patterns in cells.** A. NIH 3T3 cells were transfected with a vector encoding 3XFlag m18, 3XFlag m18L, 3XFlag m18S, or empty vector as a control. 24 hpt, cells were fixed and M18 localization was assessed by IFA using an anti-Flag antibody. Nuclei are stained with DAPI. Cells were visually evaluated for nuclear and cytoplasmic localization. Shown is a table summarizing the results. Percentages reported represent the percent of cells showing that localization pattern out of the total amount of cells analyzed for that condition. B. Shown are representative IFA images for cells transfected with each of the constructs.
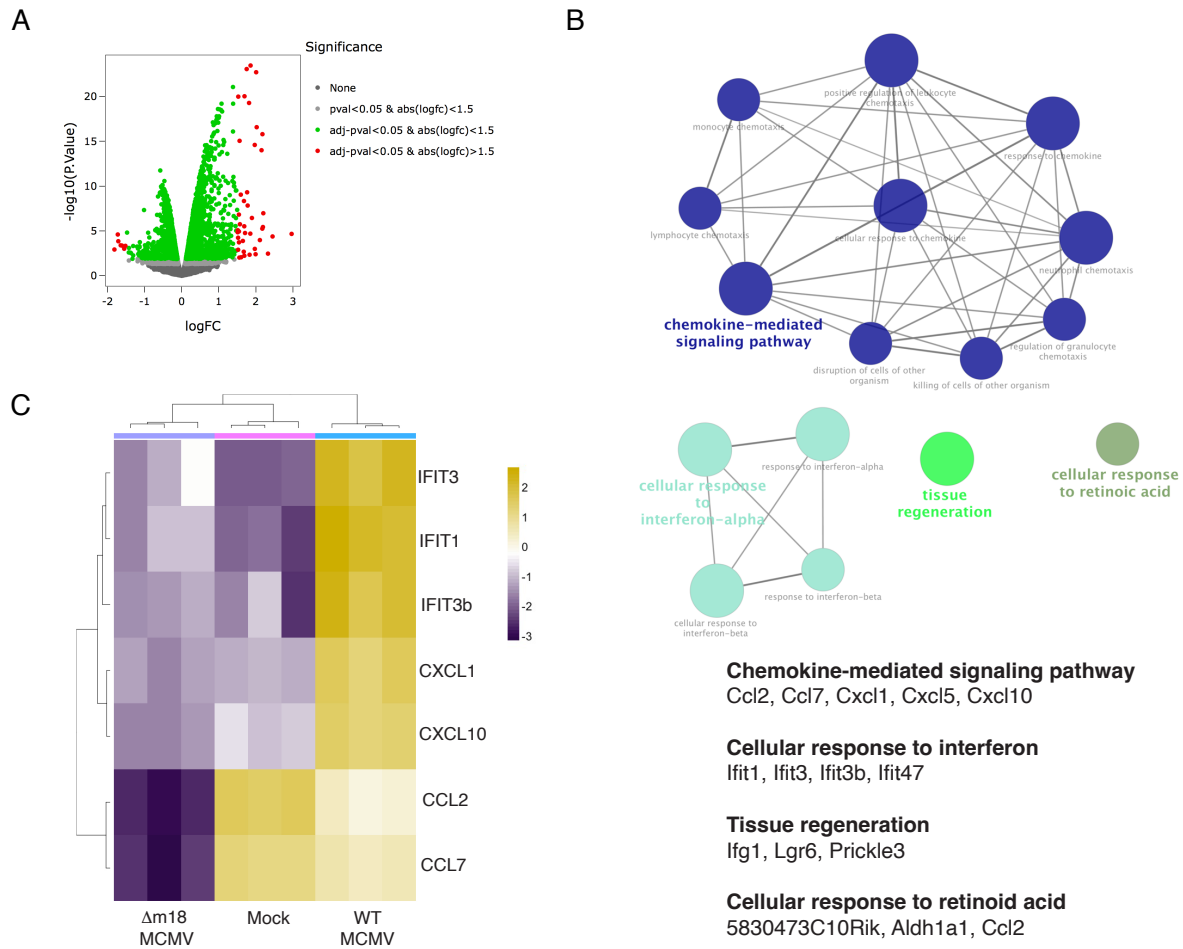
Figure 3.3: **M18 induces expression of immune-related genes.** A. NIH 3T3 cells were infected with WT MCMV, Δm18 MCMV, or uninfected (mock) as a control. 18 hpi, RNA was extracted, mRNA purified, and RNAseq was performed. Shown is a volcano plot of differentially expressed genes in cells infected with WT MCMV relative to Δm18 MCMV. Log transformed adjusted p-values (adj-pval) are shown on the y-axis and log fold change (FC) values in the x-axis. Genes with FC >1.5 and adj-pval <0.05 are shown as red dots. Genes with FC <1.5 and adj-pval <0.05 are shown as green dots. B. Gene Ontology and Pathways analysis was performed using ClueGo. Shown is a functionally grouped network highlighting pathways enriched in the top 50 differentially expressed genes in cells infected with WT MCMV vs Δm18 MCMV. Specific genes found under each category are listed. C. Heatmap showing FC expression in immune-related genes found within the top 50 differentially expressed genes. These genes were found to cluster together in the pathway analysis shown in B. Yellow represents FC increase and purple represents FC decrease.

3.4 Conclusions

The M18 protein from MCMV acts as an HDAC inhibitor by interfering with the activation of HDAC3 by CK2[108]. This inhibition relieves repression at the Rae-1 promoter and results in the transcriptional induction of these ligands. However, the presentation of Rae-1 ligands at the cell surface is blocked by virally-encoded evasins[114,115]. Since expression of ligands is detrimental to infection and MCMV directly blocks this response, we hypothesized that M18 possesses other functions.

Further characterization of M18 by Trever Greene revealed that two proteins are produced from the m18 ORF. M18L, but not M18S, was responsible for Rae-1 induction, which suggested these two isoforms might have distinct functions. Here we report that both forms of M18 are produced in cells during infection. This confirms the initial observations done using transfected cells. Furthermore, time course infection revealed that M18 is made in the initial stages of infection, as early as 4 hpi. We observed that M18S is produced first. Whether there are any functional consequences to this, or this is simply the result of more efficient translation due to M18S' smaller size, would have to be evaluated in the future.

Using IFA, we found that M18L was mainly localized to the cytoplasm, while M18S showed more nuclear localization. These results contrast with the initial observations that showed M18 localized to the nucleus. Those initial experiments were performed with C-terminally tagged fusion constructs (m18-GFP or m18-RFP), which should allow the detection of only M18L. Although the presence of GFP or RFP did not seem to interfere with the function of M18[117], it is conceivable that fusion with these fluorescence proteins could affect M18's localization, providing an explanation for the differing results. Furthermore, because the imaging on the experiment presented here was done in two planes, it is possible that the signal coming from around the nucleus (i.e. the ER) could be interpreted as a nuclear localization, particularly in cells also showing cytoplasmic localization. To deconvolute the signal coming from the nucleus versus the surrounding areas, fluorescence across the Z-plane will have to be evaluated. A confocal microscope could also improve spatial resolution and analysis in future experiments.

To gain insights into the potential functions of M18 during infection, we performed RNAseq. To our surprise, our results revealed that genes upregulated by M18 were enriched for immune factors. Specifically, various members of the IFIT family of proteins were identified. IFITs are known antiviral proteins. These proteins block translation by recognizing and binding to 2'O-unmethylated 5' guanosine mRNA cap and triphosphorylated RNA, both signs of foreign RNA[121]. A more general strategy of these proteins is to block translation by sequestering the initiation factor complex eIF3. Interestingly, induction of IFITs has also been observed in HCMV[122,123] and KSHV[124] infected cells. Knockdown of IFITs in these studies enhanced viral gene expression and viral titers, highlighting the anti-viral role of these proteins. Given this, it is unlikely that the upregulation of these factors is purposeful. In addition to IFITs, various chemokines were also found to be induced by M18. Collectively, these could mediate the recruitment of monocytes, T-cells, NK cells, and neutrophils[125,126]. Recruitment of these immune cells might be detrimental to the virus. However, HCMV and MCMV are known to hijack hematopoietic-

derived cells like monocytes for spread[127–130]. Moreover, these viruses encode chemokine and chemokine receptor homologs to attract immune cells that can aid in their dissemination[127,128,131–133]. It is conceivable then that induction of chemokines by M18 could benefit the virus. Previous data from our lab showed that M18 was required for efficient infection of the salivary glands[117]. The ability of M18 to induce chemokine expression may be connected to its ability to disseminate to the salivary glands. Future experiments should be aimed at testing this hypothesis and assessing the contribution of M18 to immune cell recruitment and dissemination *in vivo*.

3.5 Materials and Methods

Cell lines

NIH 3T3 were purchased from ATCC. Cells were cultured in DMEM (Gibco, 11995073) containing 5% FBS (VWR, 89510-186) and 1% Pen Strep (Gibco, 15140-122) at 37 °C in 5% CO_2.

Virus production and generation of mutants using BAC recombination

Dr. Caroline Kulesza provided the E. coli strain GS1783 containing MCMV pSM3fr (Fort Lewis College). The virus was amplified by infecting NIH3T3 cells at an MOI of 0.01 and allowing the infection to proceed for 5-7 days. Viral supernatant was harvested and tittered in NIH3T3 cells by TCID50.

To generate the 3XF m18 MCMV virus, E. coli strain GS1783 containing MCMV pSM3fr was used to perform markless recombination as described[134]. A DNA construct encoding 3XFm18 with homology upstream and downstream of m18 was used as template for the recombination. The incorporation of the desired mutation was confirmed by Sanger sequencing. To generate virus from this BAC, NIH 3T3 cells were transfected with 2 ug of MCMV BAC Fugene HD transfection reagent (Promega, E2311) following the manufacturer's instructions. Infection was allowed to proceed for 2 days before transferring cells to a T25 flask. Infection was allowed to proceed for 5 days, the virus was harvested and tittered in NIH3T3 by TCID50. Resulting virus was amplified, as described above.

M18 western blot

NIH 3T3 cells were infected with WT MCMV or 3XFm18 MCMV at an MOI 5. WCL was collected at 24 h or at the times specified for the time course experiment. For the blot in Figure 3.1A, cells were transfected with 2 ug of a 3XFlag m18 construct (pCMV background) using Fugene, and WCL lysate was collected 24 hpt. Briefly, cells were washed once with PBS (Gibco, 10010023) and detached using trypsin (Gibco, 25300062). Cells were centrifuged at 1,500 rpm for 8 min. The supernatant was carefully removed, and the cell pellet was resuspended in RIPA lysis buffer with Protease inhibitor and Phosphatase inhibitor. Protein concentration was determined using Pierce BCA Protein Assay Kit (Thermo Scientific, 23225) following the manufacturer's instructions. 30-40 ug of WCL was diluted in sample buffer, samples boiled for 10 min at 100 °C, and loaded into 8 % SDS-PAGE gel. After running, the gel was transferred into a PVDF membrane and blocked for 1 hr at room temperature with 5% milk in PBS. Primary and secondary antibodies were diluted in blocking buffer. Membranes were incubated with anti-FLAG M2 (Sigma, F1804; 1:1000 dilution) overnight at 4 °C. The next day, the membranes were washed 3 times with PBS for 5 min each and incubated with secondary antibody for 1 hr at room temperature. The secondary antibody used was IRDye 680RD Donkey anti-Mouse IgG (Licor, 926-68072; 1:10000 dilution). Imaging was done using an Odyssey Li-COR imager.

Immunofluorescence

NIH3T3 cells were seeded in coverslips placed inside a 6-well plate at 150,000 cells/well. Cells were transfected with 2 ug of plasmid encoding 3XFlag m18, 3XFlag m18 L, 3XFlag m18 S, or empty vector control (pCMV background). 24 hpt, cells were fixed for 15 minutes with 4% formaldehyde (Thermo Scientific, 28906) and permeabilized with methanol. Cells were blocked with a buffer containing 5% FBS and 0.3% Triton X-100 in PBS for 1 h. Anti-FLAG M2 (Sigma, F1804; 1:1000 dilution) antibody was added and cells were incubated for 2 h. Cells were then washed and incubated with Alexa Fluor 488 (Invitrogen, A21121; 1 ug/mL) secondary antibody for 1 h covered from the light. Coverslips were rinsed and then allowed to dry for 1 h covered. Coverslips were mounted using ProLong Gold antifade reagent with DAPI (Invitrogen, P36935). Slides were allowed to dry overnight before imagining on the Keyence BZ-X710.

RNAseq of MCMV-infected cells

NIH 3T3 cells were infected with WT MCMV, Δm18 MCMV, or left uninfected (mock). 18 hpi, RNA was collected using TRIzol LS (Invitrogen, 10296010), and mRNA was enriched using the Dynabeads mRNA Purification Kit (Invitrogen, 61006). RNA fragmentation, cDNA library preparation, and sequencing were performed at the Chan Zuckerberg Biohub by Laurent Coscoy. Data processing was performed by Samuel Kyobe using QuickRNAseq[135]. Genes with less than 5 reads were eliminated from the analysis. Alignment was done to the mouse genome (Mus Musculus GRCm39). Data analysis and visualization was done using START app[120]. Gene Ontology and pathways analysis was performed using ClueGo[136].

IV

Chapter IV: Conclusions

Final Summary

Millions of years of co-evolution have allowed viruses to acquire strategies directed at manipulating or co-opting every aspect of cellular biology. Studying the intrinsic link between viruses and their host has resulted in fundamental discoveries in cell biology, virology, and immunology. This dissertation focused on two aspects of cellular homeostasis and the viral proteins that disrupt these processes.

First, we turned to pH homeostasis in the secretory pathway. Maintenance of the pH gradient in the ER and Golgi is essential for its normal functioning[3,11]. Many viruses also rely on these compartments to produce their viral proteins and assemble virions. However, the acidic environment of the Golgi can be detrimental to viral fusion proteins, like SARS-CoV-2 Spike or IAV HA, that rely on regulated cleavage or conformational changes for proper functioning. In response, viruses have evolved viroporins, ion channel-like proteins capable of disturbing cellular pH gradients[4,19]. The E protein from SARS-CoV-2 functions as a viroporins by disrupting the pH of the Golgi[28]. In Chapter 2, we show that in doing so, SARS-CoV-2 E interferes with ERp44-mediated recycling of ERAAP[62]. E-mediated Golgi pH neutralization results in the loss of ERAAP protein levels and its secretion to the extracellular milieu. Two main consequences arise from changes to ERAAP's localization and function. ERAAP loss alters the peptide repertoire available for presentation to surveying CD8$^+$ T-cells[70,71]. Production of many antigenic viral peptides depends on ERAAP, which suggests that targeting this enzyme is a proper immune evasion strategy. However, ERAAP loss in mice results in the activation of QFL T-cells which can eliminate these defective cells[73,85]. QFL T-cells have not yet been described in humans and so it is possible that this strategy might still be advantageous for human viruses. The second consequence is the potential for ERAAP to modulate the host physiology. Secreted ERAAP can alter RAAS, the primary system involved in blood pressure regulation, due to its ability to cleave Ang II[92]. Although others have proposed that secreted ERAAP could play a role in COVID-19 pathology[101], to our knowledge, we are the first to show that ERAAP could be secreted from SARS-CoV-2 infected cells. Taken together, the changes caused by the loss and/or secretion of ERAAP can signal an altered cellular state, whether caused by infection or disease. This has led us to propose that ERAAP serves as a sensor of intracellular disturbances that has the potential to link cellular sensing and immune activation. This work opens a lot of questions that should represent exciting future research avenues. For example, exploring the role of ERAAP during SARS-CoV-2 infection could prove impactful in understanding COVID-19 pathology and in the development of treatments. Furthermore, investigating whether QFL T-cells exist in humans and if they could aid in controlling infections like SARS-CoV-2 would greatly expand our knowledge of how the immune system surveys and responds to cellular abnormalities.

The second aspect discussed in this dissertation is the modulation of HDACs by herpesviruses. The viral genome is heterochromatized and repressed upon arrival to the nucleus. This repression must be overcome to allow for lytic replication. In contrast, viral DNA must be repressed to transition into latency[54]. HDACs are involved in both lytic replication and latency[51]. It is thus not surprising that herpesviruses encode proteins that modulate the action of these

enzymes[58–60,137]. Chapter 3 focuses on M18, a protein from MCMV that our lab has shown functions as an HDAC inhibitor[108]. Due to the diverse roles of HDACs, M18 has the potential to modulate many different responses in the cell. My project aimed to uncover the cellular functions of M18 and its potential role in pathogenesis. Here we show that M18 exists as two distinct proteins during MCMV infection. These results confirm the initial observations done in cells transfected with m18. IFA revealed that M18L and M18S might possess distinct localizations suggesting that these isoforms have unique functions. In addition, we showed that M18 might play a role in modulating the immune response. RNAseq revealed that M18 regulates the expression of a subset of immune genes related to chemokine signaling and interferon response. These results were initially surprising as we hypothesized that M18 could alter cellular transcription to promote a pro-viral state. However, we reasoned these results might point to a role for M18 in recruiting immune cells to sites of infection to aid in dissemination[127,128,130]. M18 was shown to be required for efficient infection of the salivary glands despite being dispensable for growth in all other organs tested[117]. The salivary glands are a major site of viral persistence and shedding[118,119]. We believe these two phenotypes, M18's regulation of immune genes and requirement for salivary gland infection, are connected. A lot of effort went into deciphering the function of M18 in cells and salivary glands, but these were ultimately unfruitful. Those attempts were not discussed here as an effort to save the reader, and the writer, the frustration of discussing inconclusive experiments. Nonetheless, I believe that unraveling the role of M18 in MCMV pathogenesis is a worthy pursuit that should be facilitated by developing better and more reliable systems that could help us answer some of our more pressing questions about this enigmatic protein.

V

References

1. Beachboard, D. C. & Horner, S. M. Innate immune evasion strategies of DNA and RNA viruses. *Current Opinion in Microbiology* **32**, 113 (2016).
2. Orzalli, M. H. & Parameswaran, P. Effector-triggered immunity in mammalian antiviral defense. *Trends in Immunology* (2022) doi:10.1016/j.it.2022.10.004.
3. Kellokumpu, S. Golgi pH, ion and redox homeostasis: How much do they really matter? *Frontiers in Cell and Developmental Biology* **7**, 93 (2019).
4. Luis Nieva, J., Madan, V. & Carrasco, L. Viroporins: structure and biological functions. (2012) doi:10.1038/nrmicro2820.
5. Seto, E. & Yoshida, M. Erasers of Histone Acetylation: The Histone Deacetylase Enzymes. doi:10.1101/cshperspect.a018713.
6. Li, G., Tian, Y. & Zhu, W. G. The Roles of Histone Deacetylases and Their Inhibitors in Cancer Therapy. *Frontiers in Cell and Developmental Biology* **8**, 1004 (2020).
7. Herbein, G. & Wendling, D. Histone deacetylases in viral infections. doi:10.1007/s13148-010-0003-5.
8. Paroutis, P., Touret, N. & Grinstein, S. The pH of the secretory pathway: Measurement, determinants, and regulation. *Physiology* **19**, 207–215 (2004).
9. Collins, M. P. & Forgac, M. Regulation and function of V-ATPases in physiology and disease. *Biochimica et Biophysica Acta - Biomembranes* **1862**, (2020).
10. Marshansky, V. & Futai, M. The V-type H+-ATPase in vesicular trafficking: targeting, regulation and function. *Curr Opin Cell Biol* **20**, 415–426 (2008).
11. Khosrowabadi, E. & Kellokumpu, S. Golgi pH and Ion Homeostasis in Health and Disease. *Reviews in Physiology, Biochemistry & Pharmacology* (2020) doi:10.1007/112_2020_49.
12. Maeda, Y., Ide, T., Koike, M., Uchiyama, Y. & Kinoshita, T. GPHR is a novel anion channel critical for acidification and functions of the Golgi apparatus. *Nature Cell Biology* **10**, 1135–1145 (2008).
13. Nordeen, M. H., Jones, S. M., Howell, K. E. & Caldwell, J. H. GOLAC: An Endogenous Anion Channel of the Golgi Complex. *Biophysical Journal* **78**, 2918–2928 (2000).
14. Thompson, R. J., Nordeen, M. H., Howell, K. E. & Caldwell, J. H. A large-conductance anion channel of the Golgi complex. *Biophysical Journal* **83**, 278 (2002).
15. Rivinoja, A., Pujol, F. M., Hassinen, A. & Kellokumpu, S. Golgi pH, its regulation and roles in human disease. *Annals of Medicine* **44**, 542–554 (2012).
16. Schapiro, F. B. & Grinstein, S. Determinants of the pH of the Golgi complex. *Journal of Biological Chemistry* **275**, 21025–21032 (2000).
17. Wu, M. M. *et al.* Mechanisms of pH Regulation in the Regulated Secretory Pathway. *Journal of Biological Chemistry* **276**, 33027–33035 (2001).
18. Khosrowabadi, E. *et al.* SLC4A2 anion exchanger promotes tumour cell malignancy via enhancing net acid efflux across golgi membranes. *Cellular and Molecular Life Sciences* **78**, 6283–6304 (2021).
19. Xia, X. *et al.* Functions of Viroporins in the Viral Life Cycle and Their Regulation of Host Cell Responses. *Frontiers in Immunology* **13**, (2022).
20. Scott, C. & Griffin, S. Viroporins: Structure, function and potential as antiviral targets. *Journal of General Virology* **96**, 2000–2027 (2015).

21. Farag, N. S., Breitinger, U., Breitinger, H. G. & El Azizi, M. A. Viroporins and inflammasomes: A key to understand virus-induced inflammation. *International Journal of Biochemistry and Cell Biology* **122**, (2020).

22. Manzoor, R., Igarashi, M. & Takada, A. Influenza A Virus M2 Protein: Roles from Ingress to Egress. *International Journal of Molecular Sciences* **18**, (2017).

23. Ciampor, F. *et al.* Evidence that the amantadine-induced, M2-mediated conversion of influenza A virus hemagglutinin to the low pH conformation occurs in an acidic trans golgi compartment. *Virology* **188**, 14–24 (1992).

24. Ciampor, F., Thompson ', C. A., Grambas ', S. & Hay ', A. J. *Regulation of pH by the M2 protein of influenza A viruses. Virus Research* vol. 22 247–258 (1992).

25. Sakaguchi, T., Leser, G. P. & Lamb, R. A. *The Ion Channel Activity of the Influenza Virus M2 Protein Affects Transport through the Golgi Apparatus*.

26. Westerbeck, J. W. & Machamer, C. E. *The Infectious Bronchitis Coronavirus Envelope Protein Alters Golgi pH To Protect the Spike Protein and Promote the Release of Infectious Virus*. http://jvi.asm.org/ (2019).

27. Wozniak, A. L. *et al.* Intracellular Proton Conductance of the Hepatitis C Virus p7 Protein and Its Contribution to Infectious Virus Production. *PLoS Pathogens* **6**, e1001087 (2010).

28. Cabrera-Garcia, D., Bekdash, R., Abbott, G. W., Yazawa, M. & Harrison, N. L. The envelope protein of SARS-CoV-2 increases intra-Golgi pH and forms a cation channel that is regulated by pH. *The Journal of Physiology* **599**, 2851–2868 (2021).

29. Boson, B. *et al.* The SARS-CoV-2 envelope and membrane proteins modulate maturation and retention of the spike protein, allowing assembly of virus-like particles. *Journal of Biological Chemistry* **296**, 100111 (2021).

30. Schoeman, D. & Fielding, B. C. Is There a Link Between the Pathogenic Human Coronavirus Envelope Protein and Immunopathology? A Review of the Literature. *Frontiers in Microbiology* **11**, (2020).

31. Breitinger, U., Farag, N. S., Sticht, H. & Breitinger, H.-G. Viroporins: Structure, function, and their role in the life cycle of SARS-CoV-2. *The International Journal of Biochemistry & Cell Biology* **145**, 106185 (2022).

32. Schoeman, D. & Fielding, B. C. Coronavirus envelope protein: Current knowledge. *Virology Journal* **16**, 1–22 (2019).

33. DeDiego, M. L. *et al.* Inhibition of NF-κB-Mediated Inflammation in Severe Acute Respiratory Syndrome Coronavirus-Infected Mice Increases Survival. *Journal of Virology* **88**, 913–924 (2014).

34. DeDiego, M. L. *et al.* A Severe Acute Respiratory Syndrome Coronavirus That Lacks the E Gene Is Attenuated In Vitro and In Vivo. *Journal of Virology* **81**, 1701–1713 (2007).

35. DeDiego, M. L. *et al.* Coronavirus virulence genes with main focus on SARS-CoV envelope gene. *Virus Research* **194**, 124–137 (2014).

36. Nieto-Torres, J. L. *et al.* Severe Acute Respiratory Syndrome Coronavirus Envelope Protein Ion Channel Activity Promotes Virus Fitness and Pathogenesis. *PLoS Pathogens* **10**, e1004077 (2014).

37. Xia, B. *et al.* SARS-CoV-2 envelope protein causes acute respiratory distress syndrome (ARDS)-like pathological damages and constitutes an antiviral target. *Cell Research* 1–14 (2021) doi:10.1038/s41422-021-00519-4.

38. Bannister, A. J. & Kouzarides, T. Regulation of chromatin by histone modifications. *Cell Res* **21**, 381–395 (2011).
39. Lawrence, M., Daujat, S. & Schneider, R. Lateral Thinking: How Histone Modifications Regulate Gene Expression. *Trends in Genetics* **32**, 42–56 (2016).
40. Verdone, L., Caserta, M. & Mauro, E. D. Role of histone acetylation in the control of gene expression. *Biochem. Cell Biol* **83**, 344–353 (2005).
41. Shahbazian, M. D. & Grunstein, M. Functions of Site-Specific Histone Acetylation and Deacetylation. (2007) doi:10.1146/annurev.biochem.76.052705.162114.
42. Yang, X.-J. & Seto, E. HATs and HDACs: from structure, function and regulation to novel strategies for therapy and prevention. *Oncogene* **26**, 5310–5318 (2007).
43. Peserico, A. & Simone, C. Physical and Functional HAT/HDAC Interplay Regulates Protein Acetylation Balance. *Journal of Biomedicine and Biotechnology* **2011**, (2011).
44. Wang, Z. *et al.* Genome-wide Mapping of HATs and HDACs Reveals Distinct Functions in Active and Inactive Genes. *Cell* **138**, 1019–1031 (2009).
45. Milazzo, G. *et al.* Histone Deacetylases (HDACs): Evolution, Specificity, Role in Transcriptional Complexes, and Pharmacological Actionability. *Genes 2020, Vol. 11, Page 556* **11**, 556 (2020).
46. Louten, J. Herpesviruses. *Essential Human Virology* 235–256 (2016) doi:10.1016/B978-0-12-800947-5.00013-2.
47. Sehrawat, S., Kumar, D. & Rouse, B. T. Herpesviruses: Harmonious Pathogens but Relevant Cofactors in Other Diseases? *Frontiers in Cellular and Infection Microbiology* **8**, (2018).
48. Grinde, B. Herpesviruses: latency and reactivation – viral strategies and host response. *Journal of Oral Microbiology* **5**, 22766 (2013).
49. Cohen, J. I. Herpesvirus latency. *J Clin Invest* **130**, 3361–3369 (2020).
50. Lieberman, P. M. Epigenetics and Genetics of Viral Latency. *Cell Host and Microbe* **19**, 619–628 (2016).
51. Guise, A. J., Budayeva, H. G., Diner, B. A. & Cristea, I. M. Histone Deacetylases in Herpesvirus Replication and Virus-Stimulated Host Defense. *Viruses* **5**, 1607–1632 (2013).
52. Reeves, M. B. Chromatin-mediated regulation of cytomegalovirus gene expression. *Virus Research* (2011) doi:10.1016/j.virusres.2010.09.019.
53. Sinclair, J. Chromatin structure regulates human cytomegalovirus gene expression during latency, reactivation and lytic infection. *Biochimica et Biophysica Acta (BBA) - Gene Regulatory Mechanisms* **1799**, 286–295 (2010).
54. Liu, X., Yan, S., Abecassis, M. & Hummel, M. Biphasic Recruitment of Transcriptional Repressors to the Murine Cytomegalovirus Major Immediate-Early Promoter during the Course of Infection In Vivo. *Journal of Virology* **84**, 3631–3643 (2010).
55. Hopcraft, S. E. *et al.* Chromatin remodeling controls Kaposi's sarcoma-associated herpesvirus reactivation from latency. *PLOS Pathogens* **14**, e1007267 (2018).
56. Murphy, J. C., Fischle, W., Verdin, E. & Sinclair, J. H. Control of cytomegalovirus lytic gene expression by histone acetylation. *The EMBO Journal* **21**, 1112–1120 (2002).
57. Kuntz-Simon, G. & Obert, G. Sodium valproate, an anticonvulsant drug, stimulates human cytomegalovirus replication. *Journal of General Virology* **76**, 1409–1415 (1995).

58. Nevels, M., Paulus, C. & Shenk, T. Human cytomegalovirus immediate-early 1 protein facilitates viral replication by antagonizing histone deacetylation. *Proceedings of the National Academy of Sciences of the United States of America* **101**, 17234–9 (2004).

59. Park, J.-J. *et al.* Functional interaction of the human cytomegalovirus IE2 protein with histone deacetylase 2 in infected human fibroblasts. doi:10.1099/vir.0.83171-0.

60. Terhune, S. S., Moorman, N. J., Cristea, I. M., Savaryn, J. P. & Cuevas-Bennett, C. Human Cytomegalovirus UL29/28 Protein Interacts with Components of the NuRD Complex Which Promote Accumulation of Immediate-Early RNA. *PLoS Pathog* **6**, 1000965 (2010).

61. Reeves, M. *et al.* Autorepression of the Human Cytomegalovirus Major Immediate-Early Promoter/Enhancer at Late Times of Infection Is Mediated by the Recruitment of Chromatin Remodeling Enzymes by IE86. *JOURNAL OF VIROLOGY* **80**, 9998–10009 (2006).

62. Vargas-Zapata, V. *et al.* SARS-CoV-2 Envelope-mediated Golgi pH dysregulation interferes with ERAAP retention in cells. 2022.11.29.518257 Preprint at https://doi.org/10.1101/2022.11.29.518257 (2022).

63. Blum, J. S., Wearsch, P. A. & Cresswell, P. Pathways of Antigen Processing. *https://doi.org/10.1146/annurev-immunol-032712-095910* **31**, 443–473 (2013).

64. van de Weijer, M. L., Luteijn, R. D. & Wiertz, E. J. H. J. Viral immune evasion: Lessons in MHC class I antigen presentation. *Seminars in Immunology* **27**, 125–137 (2015).

65. Leone, P. *et al.* MHC Class I Antigen Processing and Presenting Machinery: Organization, Function, and Defects in Tumor Cells. *JNCI: Journal of the National Cancer Institute* **105**, 1172–1187 (2013).

66. Abele, R. & Tampé, R. The ABCs of immunology: Structure and function of TAP, the transporter associated with antigen processing. *Physiology* **19**, 216–224 (2004).

67. Serwold, T., Gonzalez, F., Kim, J., Richard, J. & Shastri, N. ERAAP customizes peptides for MHC class I molecules in the endoplasmic reticulum. *Nature* **419**, 480–483 (2002).

68. Saric, T. *et al.* An IFN-γ–induced aminopeptidase in the ER, ERAP1, trims precursors to MHC class I–presented peptides. *Nature Immunology 2002 3:12* **3**, 1169–1176 (2002).

69. Kanaseki, T., Blanchard, N., Hammer, G. E., Gonzalez, F. & Shastri, N. ERAAP Synergizes with MHC Class I Molecules to Make the Final Cut in the Antigenic Peptide Precursors in the Endoplasmic Reticulum. *Immunity* **25**, 795–806 (2006).

70. Hammer, G. E., Gonzalez, F., Champsaur, M., Cado, D. & Shastri, N. The aminopeptidase ERAAP shapes the peptide repertoire displayed by major histocompatibility complex class I molecules. *Nature Immunology 2005 7:1* **7**, 103–112 (2005).

71. Hammer, G. E., Gonzalez, F., James, E., Nolla, H. & Shastri, N. In the absence of aminopeptidase ERAAP, MHC class I molecules present many unstable and highly immunogenic peptides. *Nature Immunology 2006 8:1* **8**, 101–108 (2006).

72. Nagarajan, N. A. *et al.* ERAAP Shapes the Peptidome Associated with Classical and Nonclassical MHC Class I Molecules. *The Journal of Immunology* **197**, 1035–1043 (2016).

73. Nagarajan, N. A., Gonzalez, F. & Shastri, N. Nonclassical MHC class Ib-restricted cytotoxic T cells monitor antigen processing in the endoplasmic reticulum. *nature immunology VOLUME* **13**, (2012).

74. Guan, J., Peske, J. D., Taylor, J. A. & Shastri, N. The nonclassical immune surveillance for ERAAP function. *Current Opinion in Immunology* **70**, 105–111 (2021).

75. Sharpe, H. R., Bowyer, G., Brackenridge, S. & Lambe, T. HLA-E: exploiting pathogen-host interactions for vaccine development. *Clinical and Experimental Immunology* **196**, 167–177 (2019).
76. Joosten, S. A., Sullivan, L. C. & Ottenhoff, T. H. M. Characteristics of HLA-E Restricted T-Cell Responses and Their Role in Infectious Diseases. *Journal of Immunology Research* **2016**, (2016).
77. Pietra, G., Romagnani, C., Manzini, C., Lorenzo, M. & Mingari, M. C. The Emerging Role of HLA-E-Restricted CD8+ T Lymphocytes in the Adaptive Immune Response to Pathogens and Tumors. *Journal of Biomedicine and Biotechnology* **2010**, (2010).
78. Hansen, S. G. *et al.* Profound early control of highly pathogenic SIV by an effector memory T-cell vaccine. *Nature* **473**, 523–527 (2011).
79. Hansen, S. G. *et al.* Immune clearance of highly pathogenic SIV infection. *Nature 2013 502:7469* **502**, 100–104 (2013).
80. Hansen, S. G. *et al.* Broadly targeted CD8+ T cell responses restricted by major histocompatibility complex E. *Science* **351**, 714–720 (2016).
81. Hansen, S. G. *et al.* Prevention of tuberculosis in rhesus macaques by a cytomegalovirus-based vaccine. *Nature Medicine 2018 24:2* **24**, 130–143 (2018).
82. Hansen, T. H. & Bouvier, M. MHC class i antigen presentation: Learning from viral evasion strategies. *Nature Reviews Immunology* **9**, 503–513 (2009).
83. Kim, S. *et al.* Human cytomegalovirus microRNA miR-US4-1 inhibits CD8+T cell responses by targeting the aminopeptidase ERAP1. *Nature Immunology* **12**, 984–991 (2011).
84. Romania, P. *et al.* Identification of a Genetic Variation in ERAP1 Aminopeptidase that Prevents Human Cytomegalovirus miR-UL112-5p-Mediated Immunoevasion. *Cell Reports* **20**, 846–853 (2017).
85. Geiger, K. M. *et al.* Murine cytomegalovirus downregulates ERAAP & induces an unconventional T cell response to self. *bioRxiv* 2022.08.23.504566 (2022) doi:10.1101/2022.08.23.504566.
86. Tempio, T. & Anelli, T. The pivotal role of ERp44 in patrolling protein secretion. *Journal of Cell Science* **133**, (2020).
87. Hisatsune, C. *et al.* ERp44 Exerts Redox-Dependent Control of Blood Pressure at the ER. *Molecular Cell* **58**, 1015–1027 (2015).
88. Vavassori, S. *et al.* A pH-Regulated Quality Control Cycle for Surveillance of Secretory Protein Assembly. *Molecular Cell* **50**, 783–792 (2013).
89. Boson, B. *et al.* The SARS-CoV-2 envelope and membrane proteins modulate maturation and retention of the spike protein, allowing assembly of virus-like particles. *Journal of Biological Chemistry* **296**, (2021).
90. Anelli, T. *et al.* Thiol-mediated protein retention in the endoplasmic reticulum: the role of ERp44. (2003).
91. Stamatakis, G., Samiotaki, M., Mpakali, A., Panayotou, G. & Stratikos, E. Generation of SARS-CoV-2 S1 Spike Glycoprotein Putative Antigenic Epitopes in Vitro by Intracellular Aminopeptidases. *Journal of Proteome Research* **19**, 4398–4406 (2020).
92. Hattori, A. *et al. Characterization of Recombinant Human Adipocyte-Derived Leucine Aminopeptidase Expressed in Chinese Hamster Ovary Cells 1*. *J. Biochem* vol. 128 755–762 https://academic.oup.com/jb/article/128/5/755/831071 (2000).

93. Patel, S., Rauf, A., Khan, H. & Abu-Izneid, T. Renin-angiotensin-aldosterone (RAAS): The ubiquitous system for homeostasis and pathologies. *Biomedicine & Pharmacotherapy* **94**, 317–325 (2017).

94. Santos, R. A. S., Ferreira, A. J., Verano-Braga, T. & Bader, M. Angiotensin-converting enzyme 2, angiotensin-(1–7) and Mas: new players of the renin–angiotensin system. *Journal of Endocrinology* **216**, R1–R17 (2013).

95. Zhou, P. *et al.* A pneumonia outbreak associated with a new coronavirus of probable bat origin. *Nature* **579**, 270–273 (2020).

96. Scialo, F. *et al.* ACE2: The Major Cell Entry Receptor for SARS-CoV-2. *Lung* **198**, 867–877 (2020).

97. Portales, A. E. *et al.* ACE2 internalization induced by a SARS-CoV-2 recombinant protein is modulated by angiotensin II type 1 and bradykinin 2 receptors. *Life Sciences* **293**, 120284 (2022).

98. Kuba, K. *et al.* A crucial role of angiotensin converting enzyme 2 (ACE2) in SARS coronavirus–induced lung injury. *Nature Medicine* **11**, 875 (2005).

99. Augustine, R. *et al.* Increased complications of COVID-19 in people with cardiovascular disease: Role of the renin–angiotensin-aldosterone system (RAAS) dysregulation. *Chemico-Biological Interactions* **351**, 109738 (2022).

100. Gheblawi, M. *et al.* Angiotensin-Converting Enzyme 2: SARS-CoV-2 Receptor and Regulator of the Renin-Angiotensin System. *Circulation Research* **126**, 1456–1474 (2020).

101. D'amico, S. *et al.* ERAP1 and ERAP2 Enzymes: A Protective Shield for RAS against COVID-19? *International Journal of Molecular Sciences 2021, Vol. 22, Page 1705* **22**, 1705 (2021).

102. Ni, W. *et al.* Role of angiotensin-converting enzyme 2 (ACE2) in COVID-19. *Critical Care* **24**, (2020).

103. Goto, Y., Hattori, A., Ishii, Y. & Tsujimoto, M. Reduced activity of the hypertension-associated Lys528Arg mutant of human adipocyte-derived leucine aminopeptidase (A-LAP)/ER-aminopeptidase-1. *FEBS Letters* **580**, 1833–1838 (2006).

104. Kakihana, T. *et al.* Dynamic Regulation of Ero1α and Peroxiredoxin 4 Localization in the Secretory Pathway. *Journal of Biological Chemistry* **288**, 29586–29594 (2013).

105. Fraldi, A. *et al.* Multistep, sequential control of the trafficking and function of the multiple sulfatase deficiency gene product, SUMF1 by PDI, ERGIC-53 and ERp44. *Human Molecular Genetics* **17**, 2610–2621 (2008).

106. Watanabe, S. *et al.* Zinc regulates ERp44-dependent protein quality control in the early secretory pathway. (2019) doi:10.1038/s41467-019-08429-1.

107. Li, W. *et al.* MAGeCK enables robust identification of essential genes from genome-scale CRISPR/Cas9 knockout screens. *Genome Biology* **15**, 554 (2014).

108. Greene, T. T. *et al.* A Herpesviral induction of RAE-1 NKG2D ligand expression occurs through release of HDAC mediated repression. *eLife* **5**, e14749 (2016).

109. Raulet, D. H., Marcus, A. & Coscoy, L. Dysregulated cellular functions and cell stress pathways provide critical cues for activating and targeting natural killer cells to transformed and infected cells. *Immunological Reviews* **280**, 93–101 (2017).

110. Tokuyama, M. *et al.* Expression of the rae-1 family of stimulatory nk-cell ligands requires activation of the pi3k pathway during viral infection and transformation. *PLoS Pathogens* **7**, (2011).

111.   Lodoen, M. *et al.* NKG2D-mediated natural killer cell protection against cytomegalovirus is impaired by viral gp40 modulation of retinoic acid early inducible 1 gene molecules. *The Journal of experimental medicine* **197**, 1245–53 (2003).

112.   Raulet, D. H., Gasser, S., Gowen, B. G., Deng, W. & Jung, H. Regulation of Ligands for the NKG2D Activating Receptor. *Annual Review of Immunology* **31**, 413–441 (2013).

113.   Guerra, N. *et al.* NKG2D and its Ligands: 'One for All, All for One'. *Article 476 1. Immunol* **9**, 476 (2018).

114.   Jonjić, S., Babić, M., Polić, B. & Krmpotić, A. Immune evasion of natural killer cells by viruses. *Current Opinion in Immunology* **20**, 30–38 (2008).

115.   De Pelsmaeker, S., Romero, N., Vitale, M. & Favoreel, H. W. Herpesvirus Evasion of Natural Killer Cells. (2018) doi:10.1128/JVI.02105-17.

116.   Zhang, X. *et al.* Histone deacetylase 3 (HDAC3) activity is regulated by interaction with protein serine/threonine phosphatase 4. http://genesdev.cshlp.org doi:10.1101/gad.1286005.

117.   Greene, T. T. & Coscoy, L. Herpesviral Regulation of the RAE-1 Family of NKG2D Ligands. *ProQuest Dissertations and Theses* (University of California, Berkeley, 2017).

118.   Cavanaugh, V. J., Deng, Y., Birkenbach, M. P., Slater, J. S. & Campbell, A. E. Vigorous innate and virus-specific cytotoxic T-lymphocyte responses to murine cytomegalovirus in the submaxillary salivary gland. *Journal of virology* **77**, 1703–17 (2003).

119.   Cannon, M. J. *et al. Repeated measures study of weekly and daily cytomegalovirus shedding patterns in saliva and urine of healthy cytomegalovirus-seropositive children.* http://www.biomedcentral.com/1471-2334/14/569 (2014) doi:10.1186/s12879-014-0569-1.

120.   Nelson, J. W., Sklenar, J., Barnes, A. P. & Minnier, J. The START App: a web-based RNAseq analysis and visualization resource. *Bioinformatics* btw624 (2016) doi:10.1093/bioinformatics/btw624.

121.   Vladimer, G., Górna, M. & Superti-Furga, G. IFITs: Emerging Roles as Key Anti-Viral Proteins. *Frontiers in Immunology* **5**, (2014).

122.   Zhu, H., Cong, J.-P. & Shenk, T. Use of differential display analysis to assess the effect of human cytomegalovirus infection on the accumulation of cellular RNAs: Induction of interferon-responsive RNAs. *Proc Natl Acad Sci U S A* **94**, 13985–13990 (1997).

123.   Zhang, L. *et al.* Antiviral effects of IFIT1 in human cytomegalovirus-infected fetal astrocytes. *Journal of Medical Virology* **89**, 672–684 (2017).

124.   Li, D. & Sankar, S. Human IFIT proteins inhibit lytic replication of KSHV: A new feed-forward loop in the innate immune system. doi:10.1371/journal.ppat.1007609.

125.   Sokol, C. L. & Luster, A. D. The Chemokine System in Innate Immunity. http://cshperspectives.cshlp.org doi:10.1101/cshperspect.a016303.

126.   Nagarsheth, N., Wicha, M. S. & Zou, W. Chemokines in the cancer microenvironment and their relevance in cancer immunotherapy. *Nat Rev Immunol* **17**, 559–572 (2017).

127.   Daley-Bauer, L. P., Roback, L. J., Wynn, G. M. & Mocarski, E. S. Cytomegalovirus hijacks CX3CR1hipatrolling monocytes as immune-privileged vehicles for dissemination in mice. *Cell Host and Microbe* **15**, 351–362 (2014).

128.   Farrell, H. E. *et al.* Murine cytomegalovirus spreads by dendritic cell recirculation. *mBio* **8**, 1–13 (2017).

129.   Jackson, J. W. & Sparer, T. There Is Always Another Way! Cytomegalovirus' Multifaceted Dissemination Schemes. *Viruses* **10**, 383 (2018).

130.   Farrell, H. E., Bruce, K., Lawler, C. & Stevenson, P. G. Murine cytomegalovirus spread depends on the infected myeloid cell type. *Journal of virology* JVI.00540-19 (2019) doi:10.1128/JVI.00540-19.

131.   Farrell, H. E., Bruce, K., Ma, J., Davis-Poynter, N. & Stevenson, P. G. Human cytomegalovirus US28 allows dendritic cell exit from lymph nodes. doi:10.1099/jgv.0.001154.

132.   Saederup, N., Lin, Y. chun, Dairaghi, D. J., Schall, T. J. & Mocarski, E. S. Cytomegalovirus-encoded β chemokine promotes monocyte-associated viremia in the host. *Proceedings of the National Academy of Sciences* **96**, 10881–10886 (1999).

133.   Jackson, J. W. *et al.* The Human Cytomegalovirus Chemokine vCXCL-1 Modulates Normal Dissemination Kinetics of Murine Cytomegalovirus In Vivo. (2019) doi:10.1128/mBio.

134.   Tischer, B. K., Von Einem, J., Kaufer, B. & Osterrieder, N. Two-step Red-mediated recombination for versatile high-efficiency markerless DNA manipulation in Escherichia coli. *BioTechniques* **40**, 191–197 (2006).

135.   Zhao, S. *et al.* QuickRNASeq lifts large-scale RNA-seq data analyses to the next level of automation and interactive visualization. *BMC Genomics* **17**, 39 (2016).

136.   Bindea, G. *et al.* ClueGO: a Cytoscape plug-in to decipher functionally grouped gene ontology and pathway annotation networks. *Bioinformatics* **25**, 1091–1093 (2009).

137.   Gu, H. & Roizman, B. The Two Functions of Herpes Simplex Virus 1 ICP0, Inhibition of Silencing by the CoREST/REST/HDAC Complex and Degradation of PML, Are Executed in Tandem. *Journal of Virology* **83**, 181–187 (2009).